# Influence of powder particle size distribution on press–and–sinter titanium and Ti–6Al–4V preforms

Hendrik Ludolph Bosman

*Thesis presented in partial fulfilment of the requirements for the degree of Master of Engineering (Mechanical) in the Faculty of Engineering at Stellenbosch University*


Supervisor: Dr DC Blaine

March 2016

## Declaration

By submitting this thesis electronically, I declare that the entirety of the work contained therein is my own, original work, that I am the sole author thereof (save to the extent explicitly otherwise stated) that reproduction and publication thereof by Stellenbosch University will not infringe any third party rights and that I have not previously in its entirety or in part submitted it for obtaining any qualification.

Date: March 2016

## Abstract

This research focusses on the press-and-sinter manufacturing process through which titanium powders are employed to produce dense titanium and the Ti-6Al-4V alloy; more specifically, the influence of particle size distribution (PSD) on the densification behaviour and material properties are investigated.

Commercially pure (CP) titanium powders of -100 and -200 mesh sizes were blended in various proportions and used to conduct compressibility and sintering studies. To produce Ti-6Al-4V, a -200 mesh 60Al-40V master alloy (MA) powder was additionally blended with the CP titanium powders. Powders and powder blend were characterised using scanning electron microscopy and laser diffraction.

A vast array of specimens was produced while varying the following production parameters: aspect ratio, compaction pressure, sintering time and sintering temperature. Aspect ratios of cylindrical specimens were varied to produce thin disks (1:3), as well as square (1:1) and long (3:2) cylinders.

Compaction pressures were varied from 200 MPa to 600 MPa using double action compaction. Sintering was conducted under high vacuum ($<10^{-4}$ mbar, or better) with sintering temperatures ranging from 1000°C to 1300°C; typical holding times were two hours, with certain specimens being re-sintered to four, and up to six hours.

From the results of the compressibility and sintering studies, a baseline densification pathway was elected: compaction at 400 MPa followed by sintering at 1300°C for two hours. This allowed meaningful comparison of the behaviour of different powder blends. Several CP titanium and MA Ti-6Al-4V powder blends of known weight compositions were considered by creating a model using the precursor powder PSD data to predict the blended powder PSDs.

A few promising CP and MA blends were prepared and specimens were produced according to the elected baseline process. The densification behaviour was studied at each process step. Densification trends similar to those indicated in literature for bimodal powder blends were found for the CP titanium blends; however, the effect of the MA powder alloying addition was dominant in the case of the MA Ti-6Al-4V blends' densification behaviour.

Mechanical properties were tested using three point bending and Vickers hardness (HV10), respectively. Transverse rupture bar specimens were pressed (400 MPa) and showed either brittle or ductile fracture after being sintered for two hours at either 1000°C or 1300°C, respectively. The thermal conductivity of specific specimens was measured and showed that the thermal conductivity of sintered titanium is lower than

that of the equivalent wrought material. The sintered microstructure of various specimens was investigated to gain insight into differences in pore structures among the blend compositions. A vast range of densification results has been put forth from which to extract data for future research.

Recommended future work would include: the procurement of tooling for tensile test specimens, a redesign of the thermal conductivity experimental setup, and the addition of fine -325 mesh CP titanium powders to widen the range of PSDs achievable.

# Opsomming

Hierdie navorsing fokus op die pers-en-sinter poeiermetallurgiese vervaardigingsproses waardeur titaniumpoeiers gebruik word om digte titanium en die Ti-6Al-4V allooi te produseer. Meer spesifiek word die invloed van partikel grootte distribusie (PGD) op verdigtingsgedrag en materiaal-eienskappe ondersoek.

Kommersieel suiwer (KS) titaniumpoeier van -100 and -200 maasgroottes was gemeng in verskeie proporsies en gebruik in saampersbaarheid- en sinteringstudies. In die produksie van Ti-6Al-4V was ŉ -200 maas 60Al-40V meester-allooipoeier (MA) bykomend met die KS titanium poeiers gemeng. Die karaktereienskappe van die poeiers en poeiermengsels is ondersoek deur gebruik te maak van skanderings-elektronmikroskopie en laserdiffraksie.

ŉ Groot reeks monsters was geproduseer onderhewig aan die afwisseling van die volgende produksie-parameters: aspek-verhoudings, kompaksiedruk, sinteringstyd en sinteringstemperatuur. Aspek-verhoudings van silindriese monsters is afgewissel om dun skywe (1:3), asook vierkantige- (1:1) en lang-silinders (3:2) te produseer.

Kompaksie-druk is gevarieer vanaf 200 MPa tot 600 MPa met behulp van dubbelaksie-kompaksie. Sintering is uitgevoer onder hoë vakuum (<$10^{-4}$ mbar, of beter) met sinteringstemperature wat wissel vanaf 1000°C tot 1300°C met ŉ tiperende oondtyd van twee ure. Sekere monsters is hersinter tot vier, en selfs tot ses uur.

Uit die resultate van die saampersbaarheid en sinteringstudies, was 'n basislyn verdigtingspad gekies: kompaksie by 400 MPa gevolg deur sintering by 1300°C vir twee ure. Dit het die betekenisvolle vergelyking van die gedrag van verskillende poeiermengsels moontlik gemaak. Verskeie KS titanium en MA Ti-6Al-4V poeier-mengsels van gekose gewigsamestellings is oorweeg. 'n Model was geskep deur die PGD-data van die voorloperpoeier te benut om die gemengde poeiers se PGD te voorspel.

'n Paar belowende KS en MA mengsels is voorberei en monsters is vervaardig volgens die gekose basislyn-proses. Die verdigtingsgedrag is ondersoek by elke stap van die proses. Verdigtings-tendense, soortgelyk aan dié wat in die literatuur vir bimodale poeiermengsels beskryf word, is gevind vir die KS titanium mengsels. Die effek van die MA poeier se toevoeging was egter oorheersend in die verdigtings-gedrag van die MA Ti-6Al-4V mengsels.

Meganiese eienskappe is getoets met behulp van drie punt buigtoetse en Vickers hardheid (HV10), onderskeidelik. Dwars-breek balkmonsters is gekompakteer (400 MPa) en het bros óf rekbare breuk getoon na sintering vir twee

ure teen, onderskeidelik, 1000°C en 1300°C. Die termiese geleidingsvermoë van spesifieke monsters is gemeet en het getoon dat die termiese geleidingsvermoë van gesinterde titanium vêr laer is as dié van die ekwivalent smee-materiaal. Die gesinterde mikrostruktuur van verskeie monsters is ondersoek om insig te verkry oor die verskille in die poreusheid van die verskillende mengselsamestellings.

'n Groot verskeidenheid verdigtingsresultate is aangeteken waaruit data vir toekomstige navorsing onttrek kan word. Aanbevelings vir toekomstige werk sluit in: die verkryging van gereedskap vir die produksie van trektoetsmonsters; die herontwerp van die opstelling van die termiese geleidings-eksperiment; en die toevoeging van fyn -325 maas KS titaniumpoeiers om die omvang van PGDs uit te brei.

## Acknowledgements

Firstly, I would give my thanks and appreciation toward my parents, Prof HL Bosman and Mrs MW Bosman, for their continued support and encouragement during my studies.

Secondly, I would like to express my sincere gratitude toward Dr DC Blaine, my supervisor, for her support and guidance throughout my graduate and post graduate studies.

Thirdly, I would like to acknowledge the value of cooperation with the students in the SUN and UCT material science laboratories and for their camaraderie in our shared offices.

Finally, I would like to express my appreciation for the time and efforts of the SUN support staff and industry partners without whom this project would not have been possible.

# Table of contents

# List of figures

# List of tables

# Nomenclature

| | |
|---|---|
| Al | Aluminium |
| ASTM | American Society for Testing and Materials |
| BE | Blended Elemental |
| CIP | Cold Isostatic Pressing |
| CP | Commercially Pure |
| Cu | Copper |
| EDS | Energy-Dispersive X-ray Spectroscopy |
| FCC | Fray-Farthing-Chen |
| Fe | Iron |
| GA | Gas Atomized |
| GKN | Guest, Keen and Nettlefolds Sinter Metals (Pty) Ltd |
| HDH | Hydride-(mill)-Dehydride |
| HIP | Hot Isostatic Pressing |
| HV | Vickers Hardness |
| IM | Ingot Metallurgy |
| ISO | International Organization for Standardization |
| MA | Master Alloy |
| MIM | Metal Injection Molding |
| MPIF | Metal Powder Industries Federation |
| MTD | Micro Tool and Die Manufacturing Engineering (Pty) Ltd |
| NNS | Near Net Shape |
| PA | Pre-Alloyed |
| PM | Powder Metallurgy |
| PPE | Personal Protective Equipment |
| PSD | Particle Size Distribution |
| SEM | Scanning Electron Microscope |
| SMD | Stellenbosch Mechanical Services (Stellenbosch Meganiese Dienste) |
| SUN | Stellenbosch University |
| Ti | Titanium |
| TRB | Transverse Rupture Bar |
| UCT | University of Cape Town |
| V | Vanadium |
| WCVP | Western Cape Vacuum Pumps (Pty) Ltd |

# 1. Introduction

Titanium and its alloys present attractive properties as structural materials, such as superior strength to weight ratios and corrosion resistance. The Ti–6Al–4V alloy accounts for more than half of the overall titanium production with high-end applications, predominantly used in aerospace industry [1].

Despite its advantageous properties, its commercial use has been limited mainly due to production costs. This can be attributed to use of conventional ingot metallurgy (IM) to produce titanium components, the fabrication of titanium has been shown to be both difficult [2] and expensive [1]. Minimizing the amount of fabrication required is essential to promoting the use of titanium as an economically feasible structural material in a larger market, such as the automotive industry.

Thus an alternative near-net-shape approach toward the production of titanium and Ti–6Al–4V preforms will be investigated, specifically: press-and-sinter powder metallurgy (PM).

## 1.1. Motivation

Currently application of titanium and its alloys are constrained by high production costs; this has bound their use to high-end applications typically in structural parts using high grade wrought titanium alloys. The aerospace sector accounts for the bulk of the current titanium market [1]; other niche applications are found in the biomedical, automotive, armament and energy sectors [3].

These components are typically produced from ingot metallurgy (IM) techniques; refined titanium ore would be melted into ingot form which would subsequently be fabricated through a combination of forming, forging, casting and machining. These downstream processes attribute more than half of the manufacturing costs [1], as seen in Figure 1. Thus, despite their excellent material properties, these parts are not yet economically feasible for use as a structural material in the general market.

There exists an economic motive for near-net-shape (NNS) production as an alternative to the fabricated titanium parts currently in use [3]. One such process can be found in the field of powder metallurgy (PM), where metals are processed as fine (<150 µm) powders which can be consolidated and sintered to produce either finished parts or semi-finished preforms.

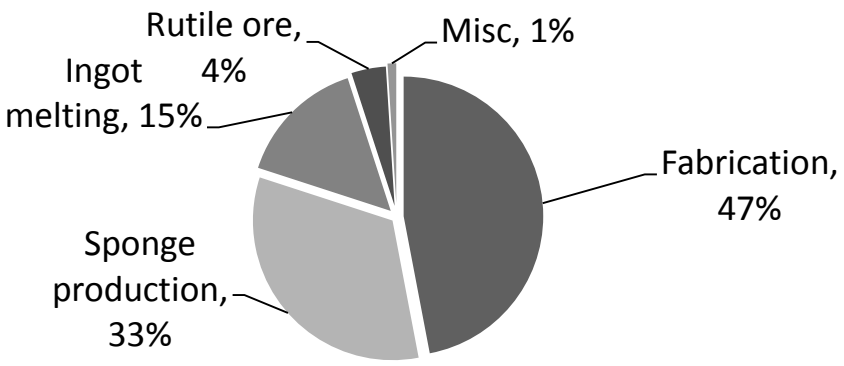


**Figure 1: Costs breakdown of conventional IM processing of titanium parts [1]**

The PM approach has two major advantages in this regard: firstly, the cost incurred in the NNS production of PM titanium parts would be less than half of the IM equivalent, and secondly, an economy of scale effect realised in larger production runs, as PM technology is geared for mass production. The commercialization of a PM process route that can produce titanium parts suited for the general market would be a significant boon to the current titanium industry [4], and would leverage titanium alloys as an economical alternative to advanced aluminium and steel alloys for use in structural components [5].

## 1.2. Objectives

The objectives for this study are to investigate and improve press-and-sinter PM processing of titanium and its alloys by:

- customising the particle size distributions of titanium and Ti-6Al-4V powder blends
- determining the influence of particle size distribution, for a range of titanium and Ti-6Al-4V powder blends, on the progression of density through each process step
- relating the densification pathways to mechanical, material and microstructural properties

## 1.3. Scope and limitations

This body of work aims to improve the production of PM titanium preforms through the conventional press-and-sinter process. Production parameters to be investigated and evaluated are powder particle size distribution, compaction pressure, specimen height, holding time and temperature during vacuum sintering.

Parameters than were left unchanged include: tooling used in compaction, vacuum conditions during sintering, heating and cooling rates during sintering. Conventional punch-and-die sets were to be used to uniaxially compact titanium powders, and vacuum conditions were not varied between sintering experiments. Material properties were investigated through a range of tests including: powder characterization, density, transverse rupture strength and hardness, microscopy and thermal conductivity.

- Powder characterization includes determining the powder morphology, shape and particle size distribution, and apparent density. Chemical analysis was not investigated beyond suppliers' chemical compositional certificates.
- Density would be determined with three distinct methods, from physical measurement for both green and sintered density; sintered density would then be compared to the Archimedes and optical density.
- Strength and hardness values would be attained through transverse rupture tests and Vickers hardness indentation, respectively.
- Microstructure would be investigated toward establishing the pore morphology in sintered specimens. Analysis of grain size and phase composition would be beyond the scope of work.
- Thermal conductivity would be measured using the experimental setup developed by Combrink [7] and Coetzer [8]

## 1.4. Development plan

The work initiated by Laubscher [9] was concluded: an investigation of CP -100 and -200 mesh HDH CP titanium powders' compaction and sintering behaviour. The influence of compaction pressure and sintering temperature on the resulting green and sintered density were to be investigated.

Further work was conducted to gain insight into the behaviour of blends consisting of these precursor powders. Toward the production of Ti-6Al-4V, a -200 mesh 60Al-40V master alloy (MA) powder was introduced [10].

The effect of a bimodal PSDs on the densification of CP titanium and MA Ti-6Al-4V were considered, thus both the prediction of PSDs of the resulting blends in addition to their compaction and sintering behaviour were to be considered.

The final round of experimentation included a combination of the previous work applied to a newly procured batch of -100 and -200 mesh CP titanium powders. Once characterized, a compaction and sintering study was conducted on these titanium powders. A range of blends was produced from CP titanium and MA precursor powders and were used in a sintering study.

The details of these experiments are delivered as follows:

- The experimental methodology has been laid out in Chapter 3 and supplemented by works procedures in Appendix A
- The execution of the each experiment has been outlined together in Chapter 4
- The experiments' results are then discussed given in Chapter 5
- Final conclusions and recommendations made can be found in Chapter 6

# 2. Literature study

The focus of the literature reviewed was aimed toward understanding what role PM titanium preforms could play in the market. Knowing the limitations of the current manufacturing techniques would allow the best application of the advantages that PM processing holds.

## 2.1. Titanium industry

This section will outline of the current interaction of processes within the titanium industry by discussing the production and refinement of titanium, the properties and application of titanium, and manufacturing techniques currently used.

The use of titanium in the pigment industry will be omitted as it can be considered irrelevant to this body of work. Although it should be acknowledged that the bulk of titanium concentrates (>90%) are consumed as pigment in the paints, paper, and medicine industries [1].

### 2.1.1. Production of titanium

Titanium oxides, in the form of rutile and ilmenite ores, are predominantly extracted in Australia, China and South Africa [11, 12]. Demand for titanium in the manufacturing industry has grown significantly in the last decade as demand in the aerospace industry continues to grow [1].

Titanium ores are traditionally refined using the Kroll or Hunter process [1, 3, 5]. These batch processes are conducted at high temperature and involve the four major steps, here follows a brief summary:

The titanium ore would be subjected to chlorination to strip the oxygen from the $TiO_2$. The product would then be distilled to remove any metallic impurities. The $TiCl_4$ is then reduced in either magnesium (Kroll) or sodium (Hunter), dependent on the process. The resulting reduction can be used to produce titanium sponge through vacuum distillation: heating the reduction in a vacuum chamber allowing the chlorinated magnesium/sodium to be extracted. This leaves a titanium sponge in the reaction vessel which can be mechanically processed into a commercially pure titanium sponge fines.

This is the first in a series of processes to produce a final component from a titanium ingot, as shown in Figure 2.

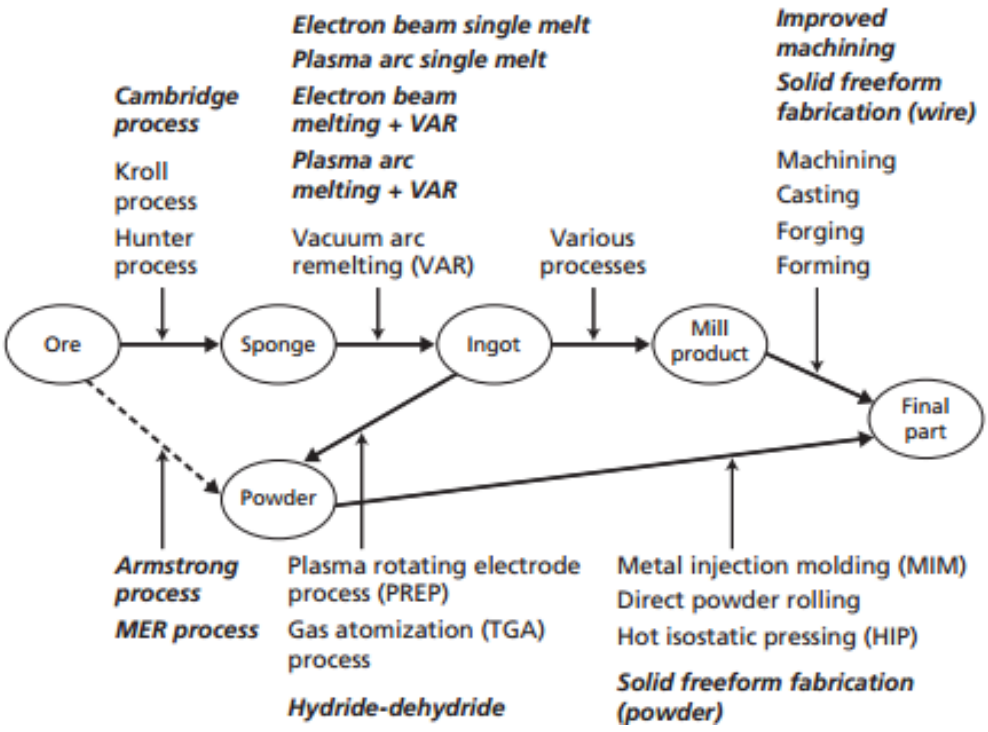


**Figure 2: Titanium production and manufacturing technologies [1]**

When these powder fines are used as a feedstock toward the ingot metallurgy (IM) process route, they typically are compacted to serve as consumable electrodes during vacuum arc remelting (VAR). Alternative melting techniques include electron beam or plasma arc melting and them followed by VAR remelts [1, 5]. These processes often make use of a cold crucible or the skull melting technique where the melt is contained inside a cooled vessel within which the melt forms a solid insulating skull around the bath [3]. From the ingot form onward a wide range of manufacturing techniques can be used to a produce a final part.

### 2.1.2. Properties of titanium

Titanium and its alloys have proven to exhibit some exceptional mechanical properties [3], especially specific strength, in addition to corrosion resistance and good biocompatibility [5]. Titanium, in its pure metallic solid form has relatively properties similar to that of copper, as shown in Table 1, however, its alloys exhibit exceptional specific strength at temperature below 500°C, as shown in Figure 3.

**Table 1: Mechanical properties of high purity Titanium, Copper and Iron [3]**

| Property | Titanium | Copper | Iron |
|---|---|---|---|
| **Elastic Modulus (GPa)** | 116 | 110 | 200 |
| **Yield Strength (MPa)** | 140 | 33 | 50 |
| **UTS (MPa)** | 220 | 210 | 540 |
| **Elongation (%)** | 54 | 60 | - |
| **Vickers hardness** | 60 | 50 | 150 |

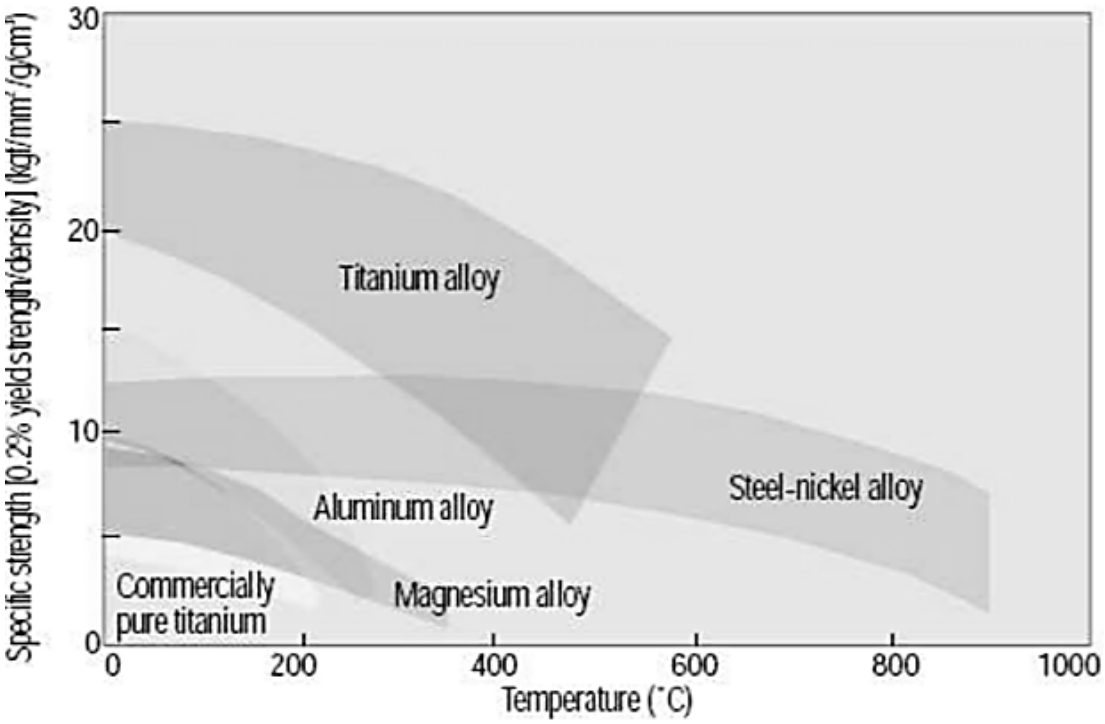


**Figure 3: Structural metals' specific strength variation with temperature [13]**

However, titanium and Ti–6Al–4V have very low thermal conductivity relative the iron and aluminium, which has a significant influence on its machinability [13]. This, coupled with the very high melting point of both titanium and Ti–6Al–4V, 1668°C and 1650°C [14], and relatively low fluidity and reactivity at high temperatures [15] has various drawbacks during IM processing [2]. Furthermore, due to its reactivity with atmospheric gases at elevated temperatures, heating and melting of titanium would typically be done under high vacuum of in an inert atmosphere.

**Table 2: Thermal conductivity of solid metals**

| Material | Conductivity at 300 K [16] | Conductivity [14] |
|---|---|---|
| **Copper** | 401 W/mK | 403 W/m.°C |
| **Aluminium** | 237 W/mK | 237 W/m.°C |
| **Iron** | 80.2 W/mK | 75 W/m.°C |
| **Titanium** | 21.9 W/mK | 22 W/m.°C |
| **Ti-6Al-4V** | - | 8 W/m.°C |

### 2.1.3. Applications of titanium

The application of titanium and its alloy have been, although rather niche, quite far reaching across may industries including: aerospace, chemical, power generation [3], oil and gas, marine, architectural, medical [15], automotive [17], armament [2]. The bulk tonnage of the application lies with aerospace and makes use of the Ti–6Al–4V alloy [1], thus it was imperative to include it in this study.

### 2.1.4. Manufacturing techniques

Predominant IM manufacturing techniques include machining, casting, forging and forming. These techniques have significant major drawbacks, the common denominator being the costs incurred to achieve an ingot or sheet product [1].

**Table 3: Cost comparison of the stages of metal production on a by volume basis [1]**

| Production stage | Steel | Aluminium | Titanium |
|---|---|---|---|
| **Metal refining** | 0.4 | 1.0 | 5.0 |
| **Ingot forming** | 0.6 | 1.0 | 10.7 |
| **Sheet forming** | 0.4 | 1.0 | 18.0 |

This cost is further escalated when considering that with the conventional IM manufacturing techniques material utilization can be as low as 10~15% [3] thus the increasing costs involved with this production route becomes evident, as shown in Figure 1. Furthermore, recycling the wasted materials on a cost effective basis has proven to be difficult [2].

## 2.2. Powder metallurgy

In this section an overview of sintering theory, powder metallurgy (PM) processes and powder production can be found.

### 2.2.1. Sintering process

Sintering is a thermal treatment for bonding particles into a solidified structure. This process occurs on small (atomic) scale through mass transport which starts adhesion of free particles leading strengthen to the structure as it tends to increase the structure's density [14].

The predominant means through with this occurs in a chemically homogenous metallic powder is solid state diffusion. To understand sintering dynamics, insight into diffusional and mass transport mechanisms must be understood. The influence of these mechanisms must be considered in order to grasp the evolution of a sintered microstructure during the different stages of sintering. Early work by Kuczynski [18] considered two stages of sintering namely, initial necking followed by pore elimination. This was expanded in subsequent work [19] to three classic stages that describes the geometric categories for analysing the sintering process, as summarized by German [14, 20], namely the initial, intermediate and final stages of sintering. The initial stage initiates neck growth with virtually no densification and coarsening. The intermediate stage is signified by pore rounding, densification and grain and pore growth. The final stage is characterized by pore closure and spheroidization, followed by and rapid grain growth with minimal densification and coarsening [21].

The experiment conducted by Alexander and Balluffi [22] shows some of the earliest evidence of the relationship between grain boundary and pore migration. They found that densification ceased once grain boundaries disappeared. This phenomenon is explained by German [14], who characterizes grain boundary diffusion as intermediate mechanism between surface and volume diffusion. In later work it was found that grain growth, grain boundary and pore migration are linked to microstructural coarsening [21].

### 2.2.2. Powder production and characteristics

There are multiple routes used in the production of PM powders, the traditional routes include chemical, electrolytic and mechanical fabrication, and atomization and evaporation techniques [20].

Mechanical means of producing powders rely on machining operations such as attaining, shearing and, ball milling and crushing. Atomization makes use of pressure applied to stream molten metal causing it disintegrate and form droplets after being exposed to either rapid cooling by an appropriate fluid, or to a centrifugal disk.

Chemical techniques exploit energetic reactions, such as thermite melting, to produce a powder as a reduction product through decomposition or precipitation whereas the electrolytic deposition requires sustained energy input to achieve similar results.

Evaporation techniques can produce nanoscale powder particle through metal vapour nucleation. These techniques produce vastly different powder types when comparing particle size and shape, cost and availability, chemistry and impurity content.

There are three classes of PM powder feedstock, namely, commercially pure (CP), pre-alloyed (PA), and blended elemental (BE), [14]. Lubricants are also used in the preparation of the PM powder, especially in the form of binders for metal injection moulding (MIM) [20].

### 2.2.3. Traditional PM techniques

Traditional press-and-sinter techniques make use of cold compaction, with either single, or preferably, double acting punch and die sets [14, 20]. Die compaction has well established and automated in industry, as the simplicity of the sequence of operation: filling, pressing compacting and ejection the green compact, leads itself well to mass production. Ejection, delamination and compaction gradients are common problems with large parts [13, 23]. Compaction pressures rarely exceeding 800 MPa, and are more commonly around 300~500 MPa [20]. After die compaction, green parts are then sintered under controlled atmosphere.

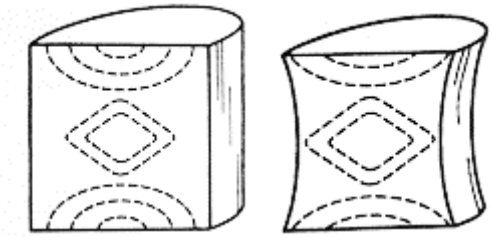

**Figure 4: Density gradients in green (left) and sintered (right) specimens [14]**

When pressing powder using uniaxial cold compaction with double action punch and die sets the green and sintered specimen exhibit density gradients which influence the densification behaviour and shrinkage as shown in Figure 4.

Pore characteristics in is influenced by the direction of compaction, as the pore shape in the green state would typically be lenticular perpendicular to the direction of compaction. However, the pore shape tends to become spherical as sintering progresses as shown in Figure 5.

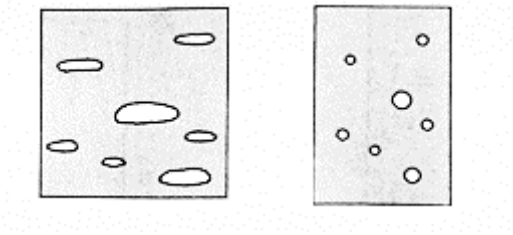

**Figure 5: Pore characteristics in green (left) and sintered (right) specimens [14]**

Sintering defects as shown in Figure 6 can induce abnormal shrinkage in the sintered specimen, which can include substrate adhesion and slumping, brought about by lack of green strength and/or excessively high sintering temperatures

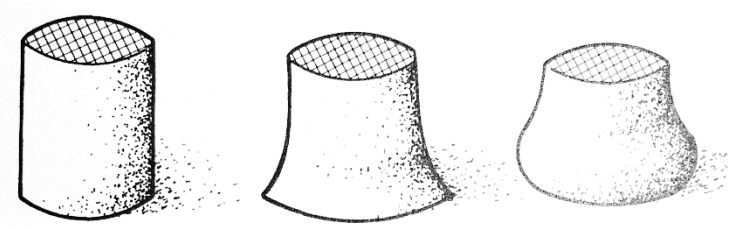

**Figure 6: Sintered specimen (left) showing defects, substrate adhesion (middle) and slumping (right) [14]**

### 2.2.4. Alternative PM techniques

Three alternatives to the traditional press-and-sinter approach will be briefly discussed, specifically: cold isostatic pressing (CIP), hot isostatic pressing (HIP), metal injection moulding (MIM) [14, 20].

CIP starts with the use of a sealed, deformable contained filled with powder. This is placed inside a pressure vessel which a hydro static pressure is applied allowing the canned powder to be consolidated. After this the green compact can be extracted and sintered.

HIP, when applied to PM manufacturing, combines the two step CIP and sinter process. This pressure assisted sintering process is similar to CIP however the container is heated and vacuum degassed prior to filling and sealing. After heating and pressure has been applied simultaneously, the sealed container can be stripped away from the sintered compact.

MIM makes use of a pelletized feedstock containing a blend of metal powders and binders (waxes, polymers and lubricants) to allow green compacts to be injection moulded. Once it has been stripped from the die the green compacted is subjected to

debinding, through either a thermal of catalytic process, to attain a brown compact to subsequently be sintered.

## 2.3. Titanium powder metallurgy

This section aims to deliver the recent developments in the application of PM techniques to the production of titanium and its alloys [24].

### 2.3.1. Titanium powder production

The Kroll and Hunter processes, described in section 2.1.1, have historically been the predominant route for the production of titanium ingots from which powder would be produced through the methods outlined in section 2.2.2. In recent years the development of specific production methods for the titanium powder has been explored.

A growing range of titanium powder are becoming commercially available, including: sponge fines (SP) from the Kroll or Hunter processes, hydride-(mill)-dehydride (HDH), gas atomized (GA), plasma rotating electrode powder (PREP) and new powders are emerging into the market from the FFC Cambridge, MER and ITP Armstrong processes' pilot plants [1,4,5,25]. General engineering use of PM titanium through mass production [26] and the use of low cost powder alternatives have been speculated [27].

### 2.3.2. PM processes for titanium production

There have been developments in the applications of PM titanium to produce NNS parts in aerospace, automotive, military and biomedical industries. The production cost of titanium components has limited its use in the automobile industry, yet it has been integrated into high-end automotive design to reduce mass and improving efficiency and performance [17]. But improvements in cold compaction and sintering techniques show great promise for the larger automotive market [3, 5]. Ti-6Al-4V compacts are typically prepared from either pre-alloyed (PA) powders or blended elemental (BE) powder blends. PA titanium powders are typically processed through HIP [24] as it has poor die compaction characteristics [3]. Two popular means of preparing BE Ti-6Al-4V powders exists [3], one involves blending three elemental powders, the other uses a blend of CP titanium and the 60Al–40V master alloy powder. When using BE three powder mixtures, special considerations must be made toward, particle size distribution, homogenization and swelling effects [10, 14]. Laser forming has also become a possible feasible option for small production runs and prototyping [28].

## 2.4. Particle size distribution effects

The effect of particle size distribution on loose packing and press-and-sinter densification has been studied [14, 29]. For solid state sintering a major determinant in the sintered density would be the initial green density. Thus understanding how to achieve better powder packing and the effect of compaction and sintering would be critical to improving densification. By blending two powders of different PSDs it is possible to attain a better packing either of the individual powders as shown in Figure 7. Furthermore, this effect is seen in the green density, but also the sintered density to a certain degree, as shown in Figure 8.

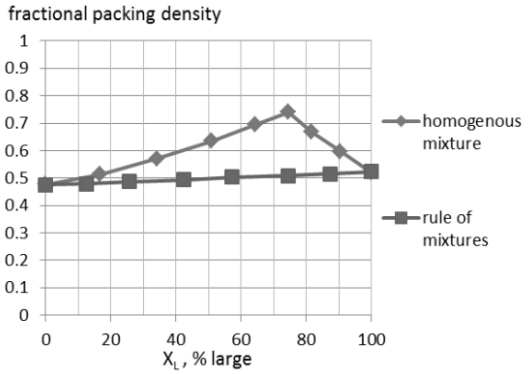


**Figure 7: Packing density variation in bimodal mixture [14]**

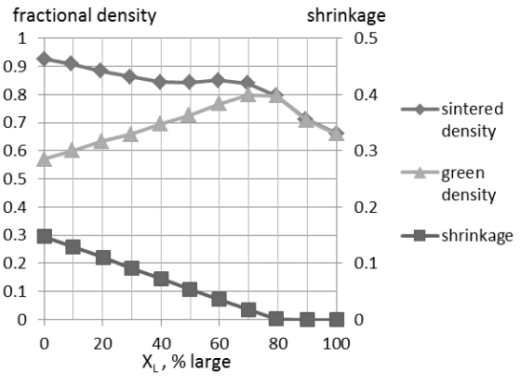


**Figure 8: Density and shrinkage plots for the sintering of bimodal iron powder (66 µm,7 µm) [14]**

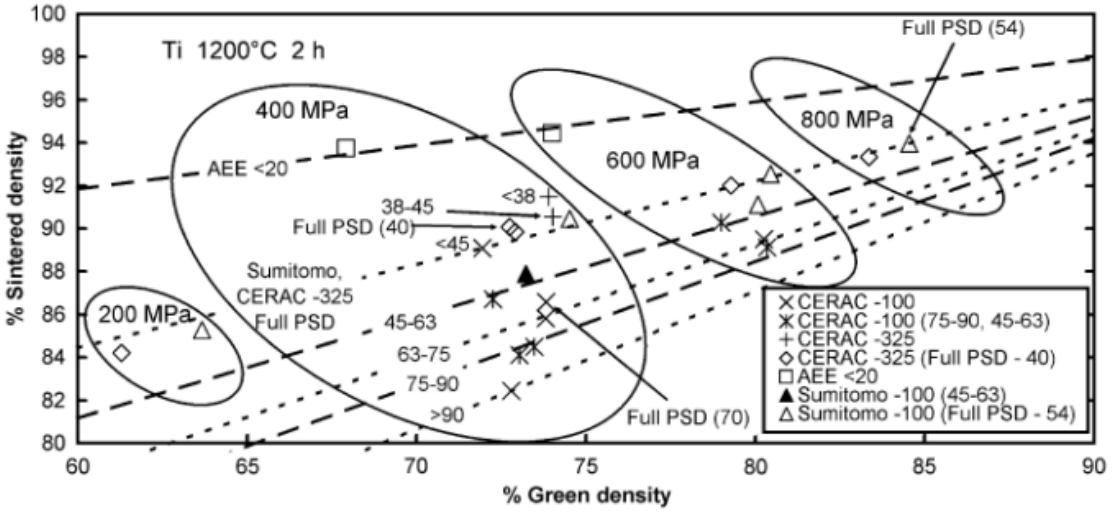


**Figure 9: Green vs. sintered density of titanium powders compacted at 200-800 MPa, [31]**

The study of the different powder particle sizes effect on the densification behaviour of PM titanium has been considered by Robertson & Schaffer [30, 31, 32]. They investigated the influence of compaction pressures, sintering time and temperatures of a range of powders.

Their research focussed on different powders from various manufacturers and different sieved fractions of those powders as shown in Figure 9. Their work illustrated that for a specific powder PSD the relation between the green and sintered densities are bound to lines of constant densification for a defined sintering cycle, as shown in Figure 9.

This research had somewhat more constraints regarding access to powder stocks. Thus an investigation was launched into the densification of CP titanium and MA Ti-6Al-4V powder blends which resulted in widened PSDs, using the approach they developed [31].

## 2.5. Overview of work conducted by Laubscher

The work conducted by Laubscher [7] looked at the press-and-sinter production parameters for PM titanium. A -100 mesh HDH titanium powder was subjected to a range of compaction pressures and sintering temperatures and the subsequent densification was monitored. Compaction and sintering practices were identified toward producing uncontaminated sintered CP titanium test specimens and relative sintered density of 91% was achieved.

Transverse rupture bar specimens were prepared with which strength testing was conducted. However, data was collected from a small amount of test specimens and further testing was recommended.

This body of work expanded the work completed by Laubscher by considering at the influence of powder PSDs effect on the press-and-sinter production process.

# 3. Experiment methodology

In order to meet the objectives of the study, as set out in section 1.2, it was necessary to design a set of powder blends, with a planned range of PSDs. These blends were then processed using the press-and-sinter techniques to produce specimens for the evaluation of the material properties at each process step.

The production and test methods that were employed throughout the study are outlined in this chapter, and supplemented by some work instructions in Appendix A. These methods are given in sequence of execution; however, the details specific to each experiment conducted would be the subject of chapter 4, and the discussions of the results and the subsequent conclusions are presented in chapter 5 and 6, respectively.

## 3.1. Powder characterization

Commercially pure (CP) titanium powders with two particle size distributions and one 60Al-40V master alloy (MA) powder were received from suppliers: Global Titanium, Alfa Aesar, and Reading Alloys, respectively. Five lots of powder were received, four CP titanium and one MA 60Al-40V powder. Throughout this document distinction between the two batches of CP titanium will be denoted by B1 and B2, as seen in Table 4. The mesh size refers to the ISO sieve size: -100 mesh indicates all particles are less than 150 µm at their largest diameter, -200 mesh indicates <75 µm [20].

**Table 4: Precursor powders, as-supplied information and designation**

| Powder | Mesh size | Batch | Production process | Supplier |
|---|---|---|---|---|
| **CP titanium*** | –100 mesh | B1 | HDH | Global Titanium |
| | | B2 | HDH | Global Titanium |
| **CP titanium*** | –200 mesh | B1 | HDH | Alfa Aesar |
| | | B2 | HDH | Global Titanium |
| **MA 60Al-40V** | –200 mesh | - | Thermite melt | Reading Alloys |

The powders' PSDs were measured using laser diffraction (Micromeritics Saturn DigiSizer). This technique measures individual powder particle sizes from the diffraction of the laser beam as it shines through a stream of suspended particles [20]. It reports the PSDs of the precursor powders in volume percentage of particle size. The discretisation interval for reporting the PSD is set by the laser diffraction equipment at $\Delta \log(\Delta D) = 0.025$, where *D* is the particle size, as-measured.

The powder morphology and chemical composition was evaluated using SEM (ZEISS EVO MA15VP) fitted with EDS (GENESIS XM2). Furthermore, apparent density and

flow rate of the titanium precursor powders was measured using a Hall flow meter and density cup with methods described in the ASTM standard [33].

## 3.2. Powder blending and PSD prediction

In order to prepare powder blends of customised PSDs, a method for predicting the PSD of a specific blend of the powders, mixed in specific peak-to-peak (mode of PSD) ratios or ratios by weight, was developed. This was achieved by taking the discretised PSD data sets of the precursor powders, weighting each according to chosen ratio, and then adding each discrete set of data points together. Thus a weighted average of the precursor PSDs was used as the blend's predicted PSD. Finally, laser diffraction particle size analysis was used to verify the actual PSD as compared to the predicted, as discussed in section 4.4.

Blending was conducted in an in-house, custom built Turbula-like mixer [13] in >100 g batches, for more detail see works procedure in Appendix A1. Note that in the description of blend composition in tables and figures the following arrangement would be used: in the case of CP titanium blends,

$$\{- -100\ mesh\ CP\ Ti\ \%wt\}:\{- -200\ mesh\ CP\ Ti\ \%wt\} \quad (1)$$

and in the case of MA Ti–6Al–4V blends,

$$\{- -100\ mesh\ CP\ Ti\ \%wt\}:\{- -200\ mesh\ CP\ Ti\ \%wt\}:\{\ 60Al - 40V\ MA\ \%wt\} \quad (2)$$

with the third value being fixed at 10%wt to achieve the required -200 mesh MA addition toward Ti-6Al-4V, although it does appear to be redundant, it would be shown for clarity.

In the light of the arrangements shown, the in text references to the blend composition would only require %wt of the -100 mesh CP titanium powder, as remaining constituents can be deduced from it.

## 3.3. Uniaxial cold compaction

Powders were uniaxially cold compacted using hardened tool steel, dual acting, free standing punch and die toolsets [6,34] as supplied and maintained by MTD. As titanium is highly reactive with hydrocarbons, especially at high temperatures, typical compaction lubricants are not mixed in with these powder blends [3].

In order to aid compaction and ejection of the part from the die, as well as to protect the tooling from wear, a die-wall lubricant of zinc stearate suspended in methanol (1 g/10 ml) was applied to the die-wall using a cotton swab [35]. This avoided delamination and cracking during part ejection and resulted in crack free green specimens [9].

All specimens were compacted in two steps, initial single action followed by final double action; detailed works procedure can be found in Appendix A2. Initial compaction was done in single action with the die supported with a spacer resting upon the bottom platen.

Final compaction was conducted with free standing toolset in the floating die position. The floating die setup enabled double action compaction, which produces a compact with greater and more homogeneous density than single action compaction [14, 20].

Depending on the cross sectional size of the specimen and the compaction pressure range required, appropriate hydraulic presses were used with the relevant tooling to produce the green compacts.

A summary of the toolsets, hydraulic presses and target pressures used in the compaction of different specimens can be found in Table 5.

**Table 5: Compaction press and toolset specifications**

| **Toolset** | **Ø10 mm cylinder** | **Ø25.4 mm cylinder** | **TRB (12.7 mm x 31.75 mm)** | **Ø36-42 mm OD stepped cylinder with Ø20 mm ID** |
|---|---|---|---|---|
| **Press** | Carver Model C manual press | Amsler hydraulic press | Amsler hydraulic press | Bussmann Simetag hydraulic press (GKN) |
| **Capacity** | 12 ton | 25 ton | 25 ton | 100 ton |
| **Target pressure** | 200-600 MPa | 400 MPa | 400 MPa | 400 MPa |
| **Compaction force** | 15.7-47.1 kN | 202.7 kN | 161.3 kN | 428.5 kN |

To account for variations in the compositions of the various powder blends and for the range of compaction pressures investigated, specimens were pressed to a target height by estimating required powder mass from attained compressibility data, and then adjusting the powder mass poured into the toolset.

This allowed sets of comparable green specimens to be produced, as green cylindrical specimens were pressed with a targeted aspect ratio (AR), defined as,

$$AR = H{:}D \quad (3)$$

where D and H represent the green specimen diameter and height, respectively.

The vast majority of specimens were produced using the 12 t Carver manual press and the Ø10 mm toolset to press three distinct shapes: long cylinders (AR=3:2), square cylinders (AR=1:1) or thin discs (AR=1:3). Compaction forces ranged from 15.7 kN to 47.4 kN to achieve the desired range of effective compaction pressures.

Transverse rupture bar (TRB) specimens was produced using a toolset designed [9] in line with ASTM [36] specifications. The load required to press at a compaction pressure of 400 MPa is 126.7 kN, and as such, the Amsler 25 ton press was used for pressing these parts. Green specimens were pressed to a thickness of ~6.7 mm, were produced by varying the mass of powder poured into the die cavity until the required thickness was achieved.

Larger, two-level, stepped cylinders were to be produced using the 36-42 mm diameter stepped cylindrical toolset with a 20 mm core rod as developed by Sobiyi [13]. Due to the high load required in order to reach a compaction pressure of approximately 400 MPa, a press capable of exerting at least 430 kN was needed to compact these rings.

To this end, a 100 ton press, housed at GKN Sinter Metals, was used to produce the green parts. The original toolset, as designed by Soybiyi [13], was modified on site to fit the machine frame. Once fitted, the Bussman press was setup to achieve a maximum cylinder pressure 50 tons which translates to maximum achievable compaction pressure of 415.4 MPa in the larger of the two stepped cylindrical sections (42 mm OD, 20 mm ID).

## 3.4. Vacuum sintering

High vacuum and high temperature sintering conditions were achieved using a horizontal tube furnace coupled to an argon supply and a two stage vacuum pump system, as supplied by Vacutech, see components listed in Table 6. The vacuum system assembly was modified to increase reliability and thus the related works procedures were also reviewed, see Appendix A3.

**Table 6: Vacuum sintering equipment list**

| Component | Manufacturer | Model | Max. operating conditions |
|---|---|---|---|
| **Horizontal tube furnace** | Elite thermal systems | Elite 1500°C, TSH 15-50-180 | Alumina tube, inner diameter 48 mm, 1500°C max temp. |

| | | | |
|---|---|---|---|
| **Rotary vane pump** | Adixen | Pascal 2012 SD | 5 x $10^{-3}$ mbar |
| **Turbo pump** | Varian | Turbo-V 81-M | 5 x $10^{-5}$ mbar |
| **Vacuum gauge** | Adixen | ACS 2000 | $10^{-6}$ mbar |

All specimens were sintered by heating at a rate of 10°C/min to the specified peak sintering temperature and holding for two hours, followed by a furnace cool to room temperature, under high vacuum conditions: $10^{-4}$ mbar or better.

Before pulling the vacuum on the furnace tube, the tube was flushed with high purity argon gas (Afrox, 99.998% pure), evacuated with low vacuum, and then flushed again before pulling the full vacuum.

The specimens were contained in yttria-stabilized zirconia crucibles during sintering (supplied by Ceratech).Yttria-stablized zirconia is recommended as a sintering substrate for titanium due to its affinity for oxygen pickup [3].

## 3.5. Density measurement

The determination of green and sintered density has been outlined in literature [6, 37] and was to be followed to as great an extent possible. Determining density from physical measurement and calculation was predominantly used and thus reported throughout this report with error bars indicating the range of the data.

Typically, mass and dimensions of the compacts were recorded to a measurement accuracy of 10 mg and 10 µm, respectively. In cases where specimens' dimensions were small, e.g. Ø10 mm x 3 mm, the measurement accuracy was increased to 10 µg and 1 µm. All calculated densities were given relative to full density titanium and Ti-6Al-4V, 4.507 g/cm$^3$ and 4.460 g/cm$^3$, respectively [14].

The calculation of specimen volume from measured values played a significant role in the accuracy of measured density [37]. Initially, some Archimedes density [38] values were captured as part of the continuation of Laubscher's work [9], but to maintain consistency throughout this document, only the measured values are reported.

A critical metric within this body of work would be the densification parameter, $\Psi$, which describes the change in density due to sintering divided by the change needed to achieve a pore free solid, i.e. full density, as defined by German [14],

$$\Psi = \frac{V_S - V_G}{1 - V_G} \tag{4}$$

where $V_g$ and $V_s$ are the fractional green and sintered densities, respectively. This

single parameter would be useful to compare the densification of powder blends which achieve a range of different green and sintered densities.

## 3.6. Mechanical testing

Strength and hardness testing were required to establish the link between the densification of titanium and Ti-6Al-4V powders, and mechanical properties of the green and sintered materials. This was evaluated through transverse rupture strength testing (3 point bend or flexural test) [6] and Vickers hardness tests [39].

### 3.6.1. Strength testing

The determination of green and sintered strength is standardised and these specifications were followed to as great an extent possible [6, 36, 40]. Transverse rupture bars (TRBs) were tested in both their green and as-sintered states using three point bending tests, as specified. Universal mechanical testing machines were used to conduct the test, the details of which are summarized in Table 7.

**Table 7: Transverse rupture test frames specification**

| TRB test | Testing frame | Load cell max. load | Crosshead travel rate |
|---|---|---|---|
| **Green strength [40]** | MTS Criterion 41 | 30 kN | 1 mm/min |
| **Sintered strength [36]** | Zwick 1484 | 200 kN | 3 mm/min |

Determination of the transverse rupture strength is specified in the standards [6] and is conducted by applying a load to the TRB, midway between supports spaced 25.4 mm apart. Thus the test is represented as a simply supported beam with a midpoint load. The yield strength and elastic modulus can be determined from the test data using simple linear elastic beam theory [39]. The bending moment, M, in the beam results in a normal stress in the beam, calculated as

$$\sigma = \frac{Mc}{I} \tag{5}$$

where the beam has a rectangular cross section with width, w and height, $2c$. The area moment of inertia is defined as $I = 2wc^3/3$. Noting that the maximum moment in the beam occurs directly below the applied load, P, and has value PL/4, where L is the distance between the supports, the transverse rupture strength is determined as

$$\sigma_{fb} = \frac{PLc}{4I} = \frac{3L}{8wc^2} P_f \tag{6}$$

where $P_f$ is the fracture load and $\sigma_{fb}$ is the transverse rupture stress (TRS).

The relationship between midpoint strain and midpoint deflection is determined by noting that the relationship between applied load, P and midpoint deflection, v, is linear

for a linear elastic material up to the point of yielding. For a brittle material, the yield and fracture point are the same for all practical purposes, as so equation (6) can be applied. For a ductile material, the linear elastic relationship is only valid up to the yield point and so alternative relationships are used to define the elastic behaviour of the material.

In the linear elastic region, the midpoint deflection is calculated according to bending beam theory as

$$\mathrm{v} = \frac{PL^3}{48EI} \tag{7}$$

Applying Hooke's law to equation (6) gives the elastic strain at the specific stress state as:

$$\varepsilon = \frac{PLc}{4EI} \tag{8}$$

Rearranging equation (7) for the midpoint deflection v to give P as a function of v, and substituting back into equation (8) yields a relationship for the strain at fracture (for brittle materials) or yielding (for ductile materials)

$$\varepsilon_{fb} = \frac{12cv}{L^2} \tag{9}$$

The standard defines ductile behaviour from a midpoint deflection, $\mathrm{v} > 0.5$ mm [6]. For ductile materials, the yield stress, $\sigma_o$ is calculated in a similar manner to the fracture stress, with the load at which 0.2% strain offset can be observed, $\mathrm{P_o}$, replacing $\mathrm{P_f}$ , in equation (5). The offset strain value is calculated using (8). Furthermore, the elastic modulus is found by applying Hooke's law to relate equations (6) and (9),

$$E = \frac{\sigma}{\varepsilon} = \frac{L^3}{48I}\frac{dP}{dv} \tag{10}$$

The slope, $\mathrm{dP/dv}$, can be derived from the initial linear portion of the captured load versus midpoint displacement curve.

### 3.6.2. Hardness testing

Vickers hardness (HV10) was measured using an EmcoTest DuraScan 10 hardness testing machine, set for a 10 kgf load. Sintered specimens were sliced axially and one half of each specimen was cold mounted in epoxy resin (Struers EpoFix), with the cut

face exposed. The mounted specimens were ground down to expose their mid plane where indentations could be made in the specimens' midpoint. Subsequently, the indentations' diagonals were to be measured using the Stream Essentials software package with images captured via Olympus GX 51 microscope fitted with a SC 30 digital camera. The Vickers hardness number can be calculated using,

$$HV = \frac{2P}{d^2}\sin\frac{\alpha}{2} \tag{11}$$

where, *d* is the average of the measured diagonals in millimetres, P is the indentation force and $\alpha$ is the indenter angle, which in this case were 10 kg and 126°, respectively [39].

### 3.7. Thermal conductivity testing

A custom-built apparatus was employed to measure the thermal conductivity of the sintered material. The original design and assembly was conducted by Combrink [7] with adaptation and improvements implemented by Coetzer [8]. On the recommendations made by Coetzer [8] the device was modified to reduce signal noise and improve measurement accuracy, with the final design shown in Figure 10. The apparatus was designed to conduct heat axially through a sintered Ø25.4 mm diameter cylindrical specimen under steady state conditions. A 600 W Ø20 mm cartridge heater was press fitted inside the copper heating probe (Ø25 mm) and powered by a 60 V DC power supply. Heat generated in this probe would be conducted through the specimen along to the copper cooling probe to which an aluminium heat sink with a CPU cooling fan is attached in order to provide a temperature drop over the assembly. Thermocouples would measure the temperature 5 mm before and 5 mm after the heating probe-specimen interface ($T_1$ and $T_2$, respectively), and then 5 mm before and 5 mm after the specimen-cooling probe interface ($T_3$ and $T_4$, respectively). The temperature is also measured at a specified length, $L_c$ = 25 mm, further along the cooling probe, location $T_5$. The data acquisition unit and thermocouples used were Eagle µDAQ Temperature unit USB-73T, and type K thermocouples in Ø1.5 mm probes.

A heat conduction diagram, representing the flow and losses in the apparatus, can be seen in Figure 11. The assembly is insulated at its outer diameter from just before the heating probe-specimen connection to the end of the cooling probe with insulating wool, incorporating measurement points $T_2$ to $T_5$. Thermal contact paste (Unick, $k_c$ = 0.9W/m.K) is used to minimize contact losses at the probe-specimen connections. Nevertheless, as the heat loss from the exposed section of the heating probe and contact losses at the connection points cannot be accurately quantified, thus

measurement points on the cooling probe were used to quantify the heat flow during each test once steady state conditions had been reached.

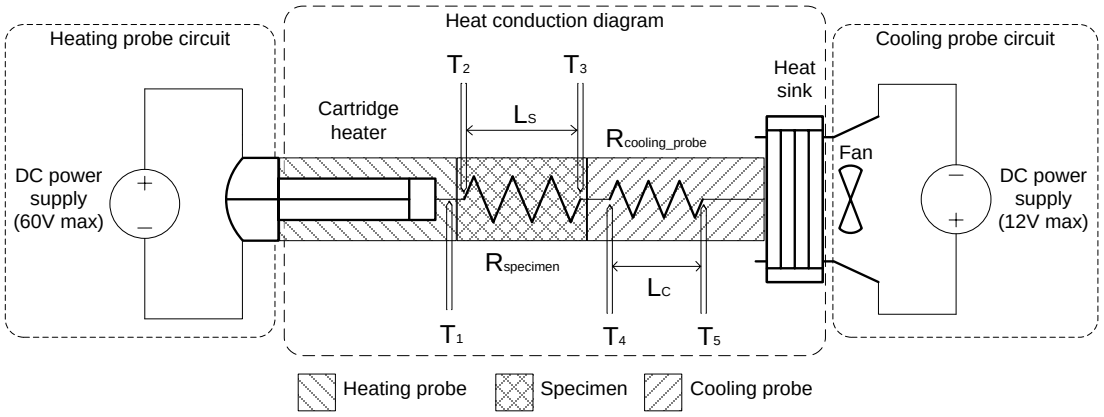


**Figure 10: Diagram of thermal conductivity test apparatus**

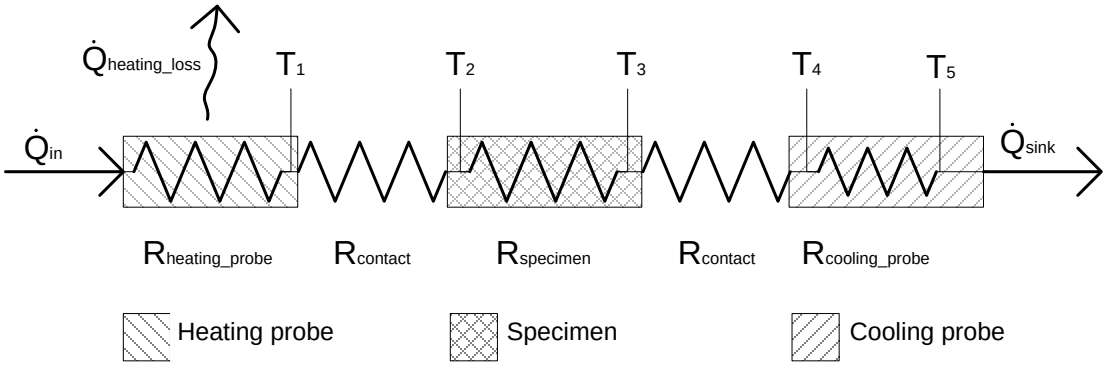


**Figure 11: Heat conduction diagram**

Assuming that there is minimal radial heat loss between measurement points $T_2$ and $T_5$, at steady state conditions, the heat flow rate through the specimen and cooling probe is calculated using the one-dimensional heat conduction equation [16],

$$\dot{Q}_{cond} = -kA\frac{dT}{dx} \tag{12}$$

where the thermal conductivity, $k$, can be estimated if the temperature gradient, $dT/dx$, through a conductor of a known cross sectional area, $A$, is known. Heating losses from the heating probe to atmosphere were unavoidable, thus determining the heat flow entering the heat conduction circuit would be challenging to quantify. However, as

conductivity of the cooling probe is known ($k_{Cu}$=401W/mK, see Table 2), thus, one-dimensional linear heat flow from $T_2$ to $T_5$, the heat flow rate can be approximated though the discrete form,

$$\dot{Q}_{sink} = -k_{Cu} A_c \frac{T_5 - T_4}{L_c} \tag{13}$$

where $L_c$ is the distance between the thermocouples on the cooling probe ($T_4$, $T_5$) and $A_c$ is the associated cross-sectional area. The assumption that with at steady state conditions the system the heat flow rate is assumed to be the same in the specimen and the cooling probe are alike. The thermal conductivity of the specimen would then calculable by rearranging the one-dimensional heat conduction equation and applying it over the specimen between points $T_2$ and $T_3$, and using the now known heat flow,

$$k_{specimen} = \dot{Q}_{sink} \frac{A_s}{L_s(T_2 - T_3)} \tag{14}$$

where, $L_s$ is the distance between the thermocouples on the specimen ($T_2$, $T_3$) and $A_s$ is the associated cross-sectional area of the specimen.

## 3.8. Microscopy

The sintered microstructures were characterised using optical light microscopy. Specimens from the first batch of titanium powders (B1), the cylindrical sintered specimens were sectioned along their longitudinal axis using a diamond blade in a low speed precision saw with cooling lubricant. These specimens were cold mounted in epoxy resin (Struers EpoFix) and allowed to at room temperature for cure overnight. Conversely, thin disc specimens prepared from the second batch of titanium powders (B2) were mounted on the cross sectional surface and subsequently ground down to expose the midplane.

The mounted specimens' exposed surfaces were ground and polished according to standard metallographic procedures prescribed for wrought titanium [41, 42] and PM metals [42, 43]. To reveal the sintered pore structure in the as-polished state free of residual abrasive scratch marks or friction induced smearing, great care had to be taken during rough polishing with was conducted using a 9 µm diamond suspension on a resin bonded diamond grinding disc. All images where gathered with using the Stream Essentials software package via Olympus GX 51 microscope fitted with a SC 30 digital camera.

# 4. Experiment results

A range of experiments were completed, with specimens produced from both batches of CP titanium precursor powders (B1, B2), toward investigating the influence of particle size distribution on the press-and-sinter behaviour of titanium and Ti-6Al-4V powder blends. These included: characterization of precursor powders, compaction and sintering studies, blend prediction and preparation, and microscopy. The supply of the first batch of precursor titanium powders had been depleted at this stage, thus only the second batch's mechanical and further material properties could be found. The data points and the related error bars shown in this chapter represent an average and range, respectively, of a minimum of three specimens' results; the single specimen thermal conductivity tests were only exception in this regard.

## 4.1. Characterisation of precursor powders

The powders used in this study were introduced in section 3.1, see Table 4. All powders were analysed in their as received state without sieving or additives. Precursor powders' particle size distributions (PSDs) were found using laser particle size analysis as described in section 3.1. The data points are shown for PSD volume frequency plots, Figure 12 and Figure 14, but they are omitted for clarity on the cumulative plots, Figure 13 and Figure 15, respectively. The -200 mesh MA powder repeated for comparison only.

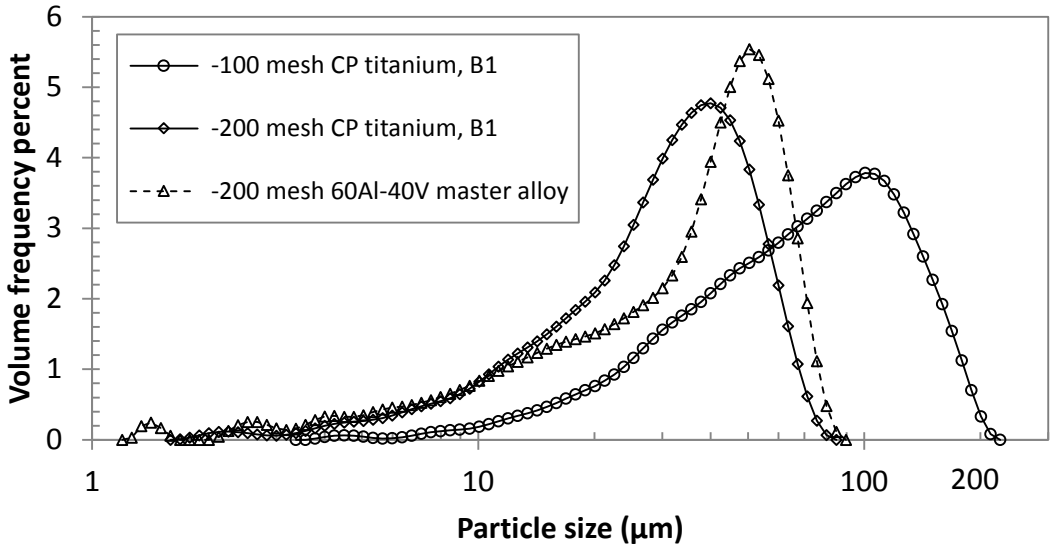


**Figure 12: Particle size distributions of precursor powders, B1**

Note the logarithmic scale on the horizontal axis, also the -200 mesh distributions are roughly log-normal [20] with a significant component of sub-sieve powder (<35 µm), however the -100 mesh distribution (CP titanium) are broad and larger than expected (>150 µm).

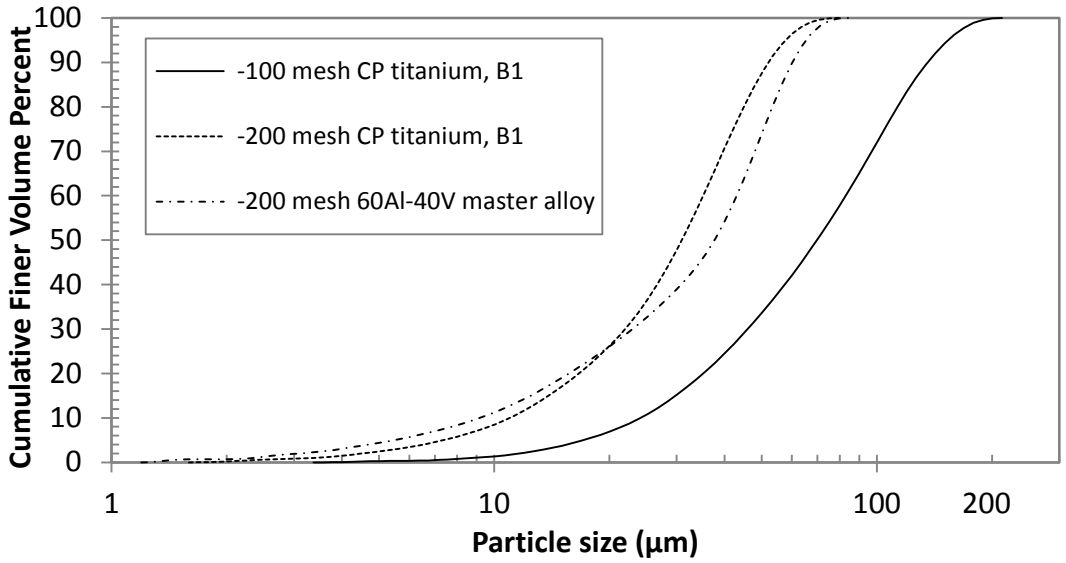


**Figure 13: Cumulative particle size distributions of precursor powders, B1**

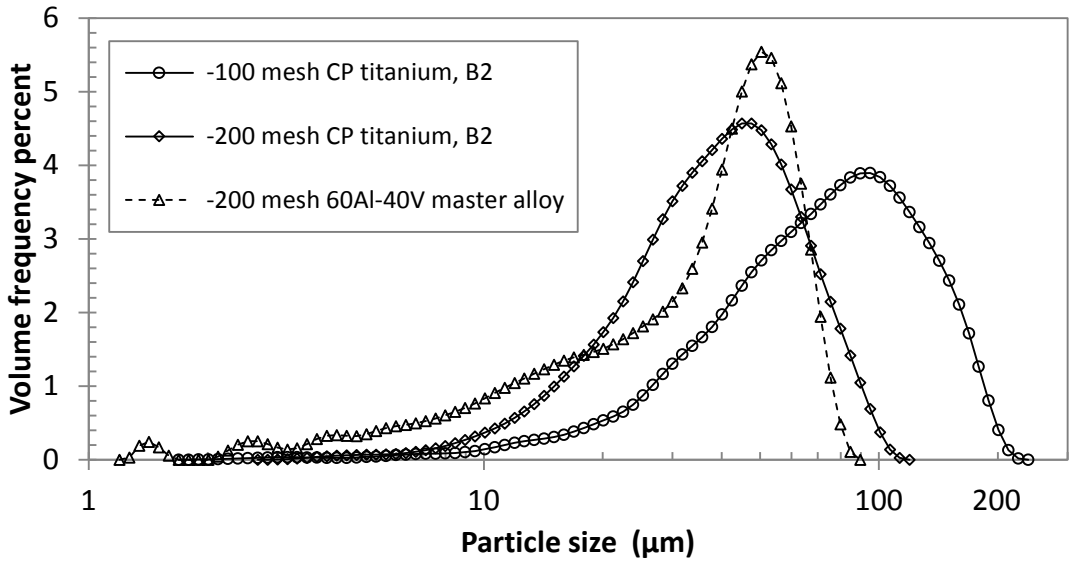


**Figure 14: Particle size distributions of precursor powders, B2**

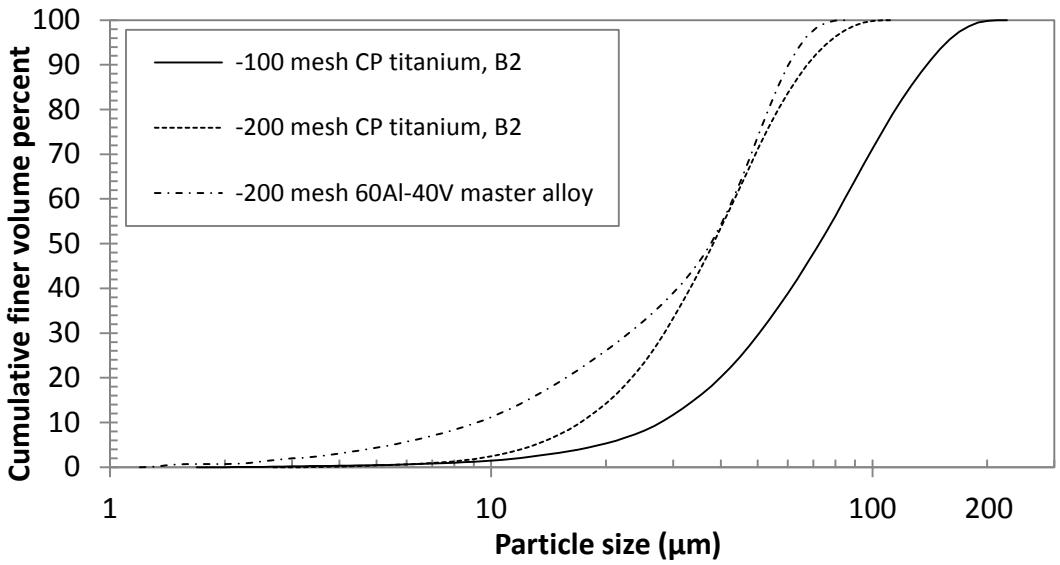


**Figure 15: Cumulative particle size distributions of precursor powders, B2**

The particle size analysis volume frequency percent data sets were used to find the mode particle sizes, similarly the cumulative finer data sets were reworked to the %finer particle sizes for D10, D50 and D90 values. Note the -100 mesh and -200 mesh powders' modes are designated $X_L$ and $X_S$, respectively.

**Table 8: Precursor powders' $D_{10}$, $D_{50}$, $D_{90}$ and mode particle sizes**

| Precursor powder (batch) | $D_{10}$ (µm) | $D_{50}$ (µm) | $D_{90}$ (µm) | Mode $X_S$ | Mode $X_L$ |
|---|---|---|---|---|---|
| **-100 mesh CP Ti (B1)** | 24.2 | 69.8 | 135.9 | - | 100.6 |
| **-100 mesh CP Ti (B2)** | 27.8 | 72.5 | 138.8 | - | 95.0 |
| **-200 mesh CP Ti (B1)** | 11.0 | 30.9 | 52.2 | 40.1 | - |
| **-200 mesh CP Ti (B2)** | 17.1 | 38.2 | 67.5 | 44.9 | - |
| **-200 mesh 60Al-40V MA** | 9.2 | 37.6 | 60.2 | 50.4 | - |

The particle morphology of raw powder was investigated using SEM imaging together with chemical analysis of green compacts using EDS, as reported in Table 9 and Table 10, respectively. Particle shape was found to be angular with the larger particles were irregular. Apparent density measurement of CP titanium precursor powders was attempted with a Hall flow meter but the powders did not flow. However the second batch of titanium powders (B2) were poured into the density measuring cup [33] with a large funnel (Ø7 mm orifice) and the -100 and -200 mesh powder's relative apparent densities were approximated at 29.1% and 25.6%, respectively. See section 3.5 for theoretical density of titanium used in this calculation.

**Table 9: SEM micrographs showing morphology of precursor powders**

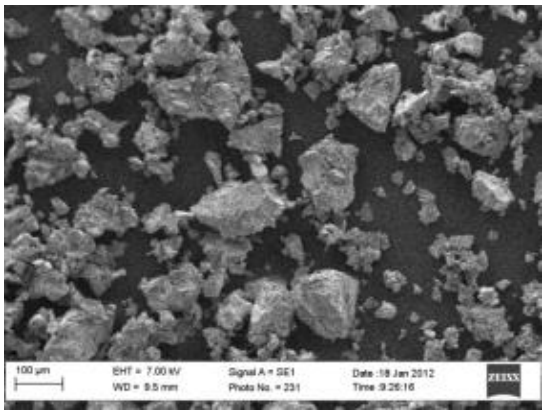

**Figure 16: Morphology of -100 mesh CP titanium powder, B1**

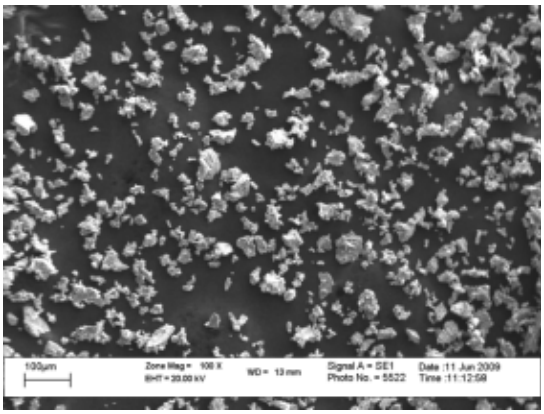

**Figure 17: Morphology of -200 mesh CP titanium powder, B1**

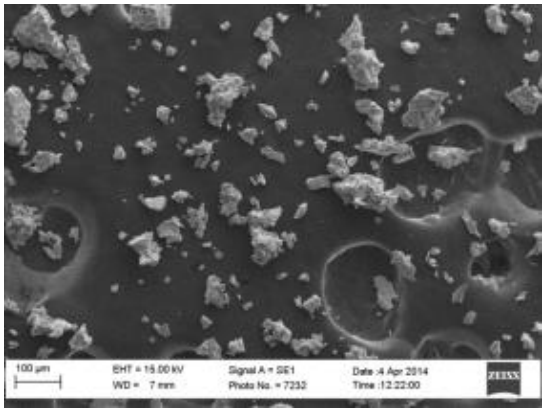

**Figure 18: Morphology of -100 mesh CP titanium powder, B2**

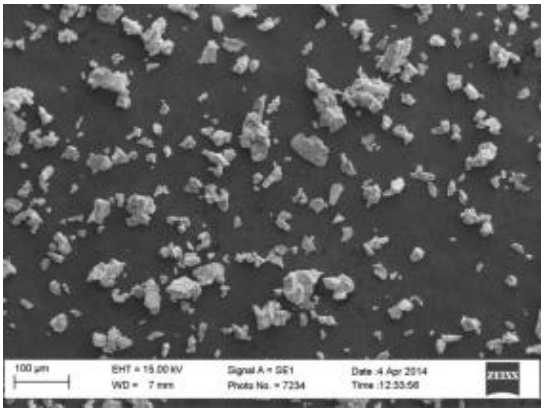

**Figure 19: Morphology of -200 mesh CP titanium powder, B2**

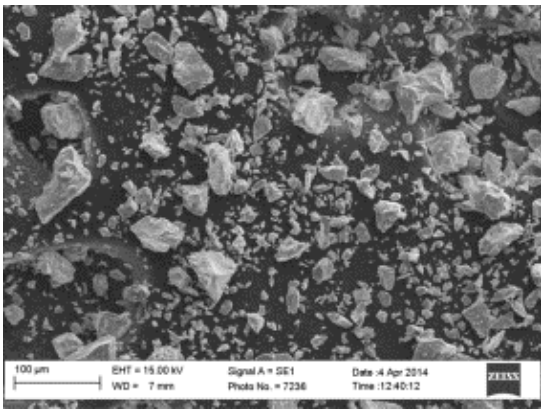

**Figure 20: Morphology of -200 mesh MA 60Al-40V powder**

**Table 10: SEM micrographs of precursor powder green compacts (compaction pressure 400 MPa) and EDS spot analysis or supplier's chemistry data**

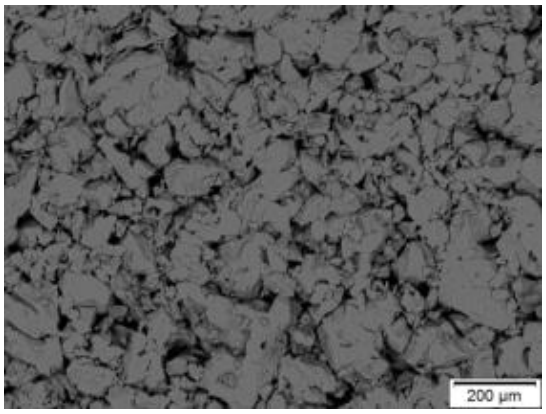


**Figure 21: Green compact -100 mesh CP titanium, B2**

Chemical data as determined with EDS:

| | |
|---|---|
| Titanium | > 99.8% |
| Aluminium | trace |

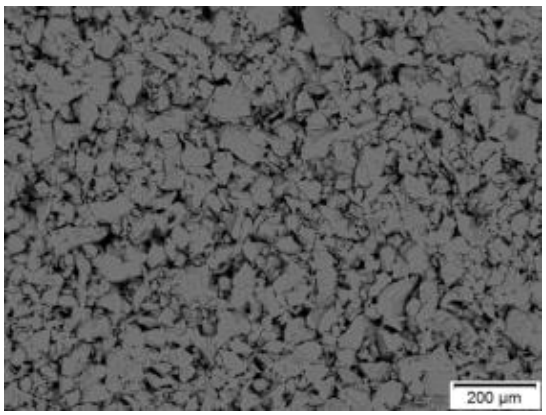


**Figure 22: Green compact -200 mesh CP titanium, B2**

Chemical data as determined with EDS:

| | |
|---|---|
| Titanium | > 99.8% |
| Aluminium | Trace |

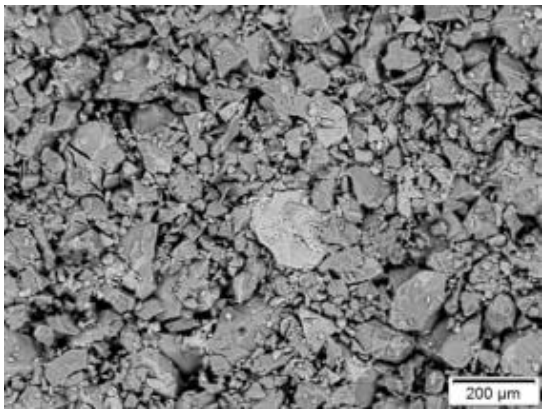


**Figure 23: Green compact -200 mesh MA 60Al-40V**

EDS results were spurious and thus omitted, chemistry data from supplier:

| | |
|---|---|
| Aluminium | 54-60%wt |
| Vanadium | 40-45%wt |
| Boron | 0.003%wt Max. |
| Carbon | 0.10%wt Max. |
| Chromium | 0.20%wt Max. |
| Copper | 0.10%wt Max. |
| Iron | 0.50%wt Max. |
| Magnesium | 0.05%wt Max. |
| Manganese | 0.05%wt Max. |
| Molybdenum | 0.30%wt Max. |
| Nickel | 0.05%wt Max. |
| Phosphorus | 0.02%wt Max. |

## 4.2. Compressibility of precursor titanium powders

A set of Ø10 mm green specimens were pressed from both batches of CP titanium powder at a range of compaction pressures with the resulting compressibility data shown in Figure 24 and Figure 25. For the first batch of powders (B1), the specimen's aspect ratio of 3:2 was prescribed as it was a continuation of the work of Laubscher [9]. For test specimens produced from the second batch of precursor powders (B2), the aspect ratio was reduced to 1:3 to more closely represent the specimens described the uniaxial compressibility test standards [35].

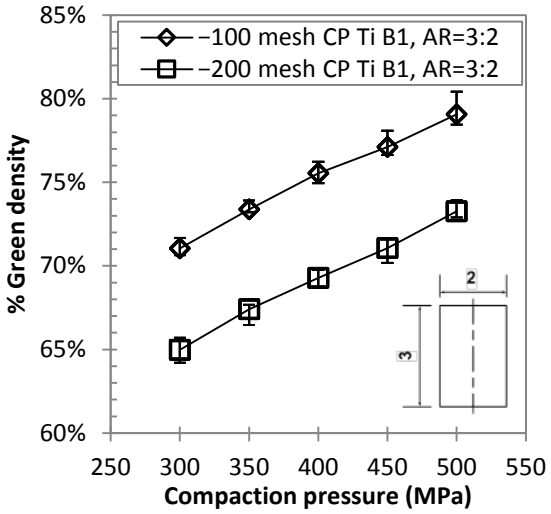


**Figure 24: Compressibility of precursor CP titanium powders, B1, AR=3:2**

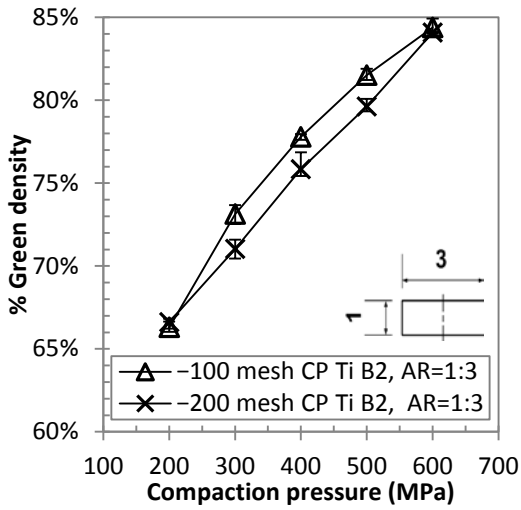


**Figure 25: Compressibility of precursor CP titanium powders, B2, AR=1:3**

Note that the changes range of compaction pressures was expanded from 300-500 MPa to 200-600 MPa and the compaction pressure increments increased from 50 to 100 MPa for the first and second powder batches (B1, B2), respectively.

## 4.3. Sintering of precursor titanium powders

The titanium precursor powders' densification behaviour through press-and-sinter processing was investigated. This would serve to establish suitable production parameters for further experiments but also as baseline to which the densification of powder blends could be compared. A study of compaction pressure and sintering temperature Laubscher [9] was expanded, the compaction pressure and sintering time was subsequently considered.

### 4.3.1. Effect of sintering temperature

The continuation of the work resulted in an expanded study of -100 mesh and further to include -200 mesh titanium precursor powders (B1), specifically influences of compaction pressure and sintering temperature on densification. Test specimens of Ø10 mm were pressed at 300-500 MPa to an approximate aspect ratio of 3:2. The green specimens were then sintered under high vacuum at sintering for two hours at temperatures of 1100°C, 1200°C and 1300°C, respectively, as shown in Figure 26.

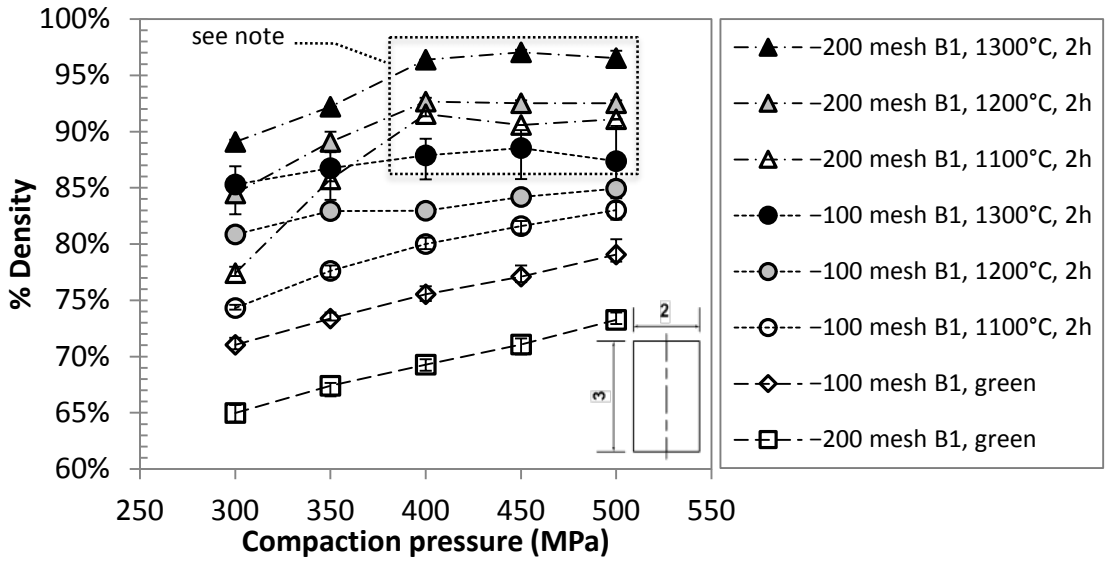


**Figure 26: Compaction pressure and sintering temperature study of CP titanium precursor powders, B1, AR=3:2**

Note the CP titanium compacts in Figure 26 show a steady increase in sintered density with an increase of either compaction pressure or sintering temperature; however, this was not evident for -200 mesh compacted at and above 400 MPa at all three sintering temperatures or the -100 mesh compacted at and above 400 MPa and sintered at 1300°C.

### 4.3.2. Effect of sintering time

Further work was completed with -100 and -200 mesh titanium precursor powders (B2), specifically the influence compaction pressure and sintering time on densification was considered. Test specimens of Ø10 mm were pressed at 200-600 MPa to an aspect ratio of 1:3. The green specimens were then sintered under vacuum in two hour segments at 1300°C for total sintering times of 2, 4 and 6 h, respectively, as shown in Figure 27.

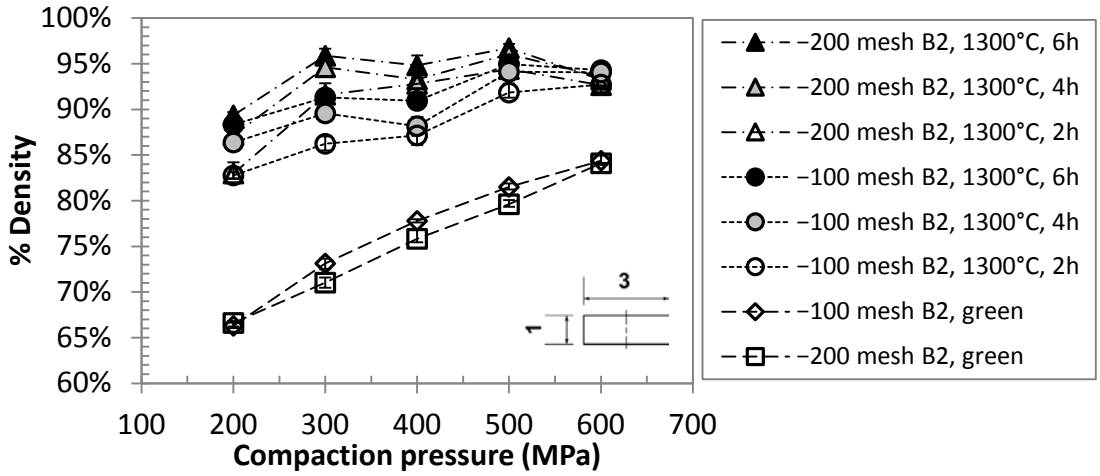


**Figure 27: Compaction pressure and sintering time study of CP titanium precursor powders, B2, AR=1:3**

## 4.4. Powder blend prediction and measurement

Having attained the PSDs of precursor powders (see section 4.1), it became possible to predict a blend's PSD for a known by weight ratio of precursor powders. This was done by using the PSD data sets of said precursor powders, weighting each according to the chosen ratio and then adding them together to achieve a weighted average, as explained in section 3.2.

This method required some form of verification though measurement [20]. To this end the -100 mesh and -200 mesh CP titanium powders (B1) were combined on a 50:50%wt basis to serve as a test blend. This blend was sampled and the PSD found using laser particle size analysis which was compared to the predicted result.

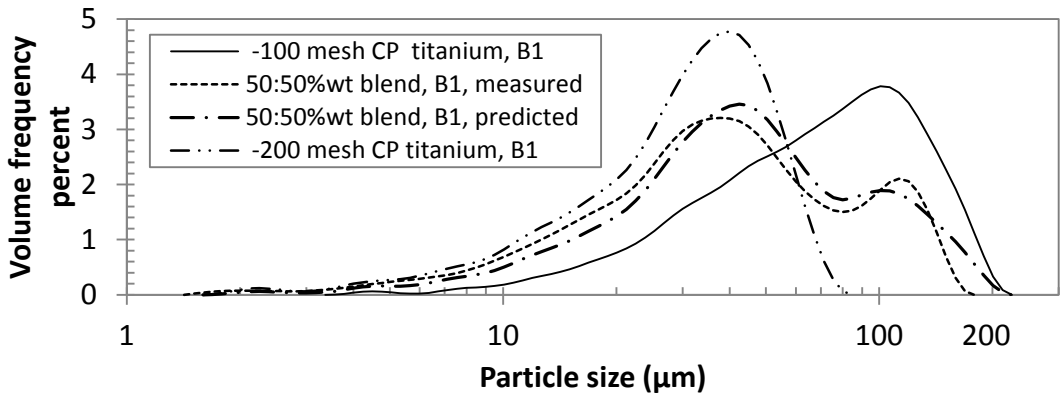


**Figure 28: Predicted and measured PSD of 50:50%wt titanium test blend, B1**

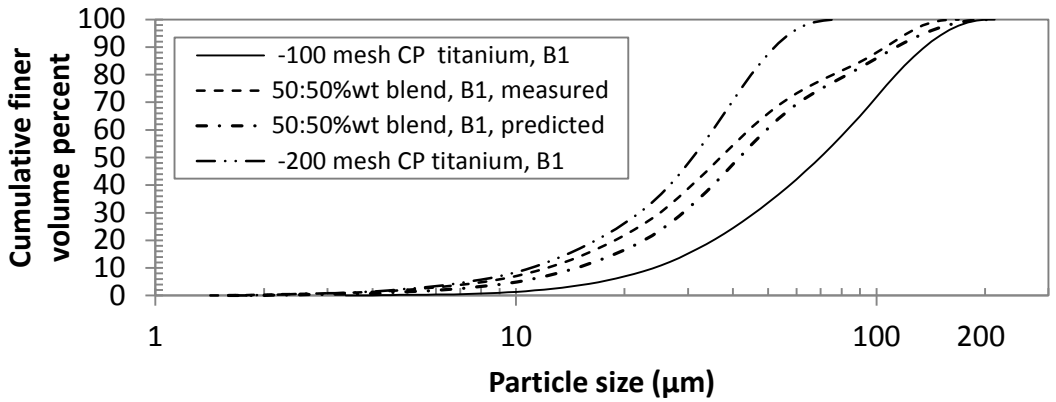


**Figure 29: Predicted and measured cumulative PSD of 50:50%wt titanium test blend, B1**

Although the predicted PSD would be analytically correct, initial errors in the measurement of precursor PSDs, sampling error and particle shape effects on the automated size analyser's measured PSD are significant.

Repeatability of successive tests with same powder and instrument are known to be within 0.5% and a cumulative error of ±4% [20] can be expected regarding the median particle size; this holds true if the results shown in Figure 28 and Figure 29 are scrutinized.

Taking these matter into account, it is important to note that the blends' predicted PSDs and modal values in this body of work are shown as estimates for comparative purposes, especially for the MA Ti-6Al-4V blends, however, the by weight composition would be accurate for both the CP and MA blends. Hence the prediction method be taken as sufficiently accurate for the purposes of comparison, and was utilized in sections 4.5 and 4.6.

## 4.5. Preparation of CP titanium powder blends

The first round of CP titanium blends (B1) were tailored to have specific frequency percent ratios between the mode values, i.e. the PSD's local peaks, $X_L$ / $X_S$, were specified ratios specifically 1 / 1, 2 / 3, and 1 / 3.

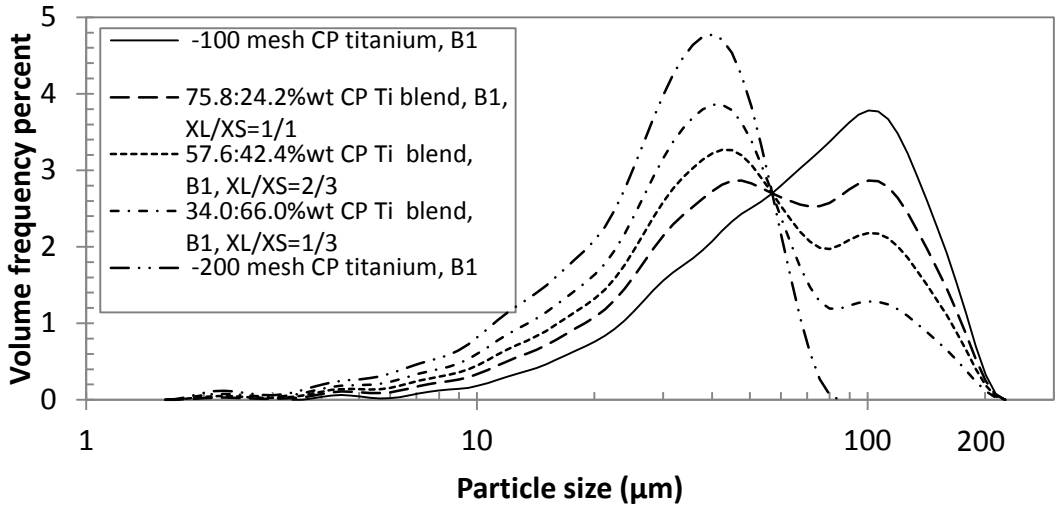


**Figure 30: PSDs of CP titanium blends, B1**

Note that as the %wt -100 mesh increases the $X_S$ peak shifts to the right, i.e. the mode value $X_S$ would be found at a slightly larger particle size, as found in Figure 30 and Table 11. This is due to the -100 mesh CP titanium precursor powder overlaps -200 mesh CP titanium.

Contrary, the $X_L$ peak does shift with the addition of -200 mesh as the PSD does include particles of that size.

**Table 11: CP titanium blends' PSD characteristics, B1**

| %wt | $D_{10}$ (µm) | $D_{50}$ (µm) | $D_{90}$ (µm) | Mode $X_S$ | Mode $X_L$ | Freq. $X_L$ / $X_S$ f |
|---|---|---|---|---|---|---|
| **0:100%wt** | 11.0 | 30.9 | 52.2 | 40.1 | - | - |
| **34.0:74.0%wt** | 13.2 | 37.2 | 98.0 | 42.4 | 100.6 | 1 / 3 |
| **57.6:42.4%wt** | 15.6 | 44.5 | 118.3 | 42.4 | 100.6 | 2 / 3 |
| **75.8:24.2%wt** | 18.4 | 60.6 | 127.4 | 47.6 | 100.6 | 1 / 1 |
| **100:0%wt** | 24.2 | 69.8 | 135.9 | - | 100.6 | - |

Note: The blends' particle sizes were predicted using precursor powders' measured PSD data.

The second round of blends prepared (B2) was chosen purely on a by-weight basis using 25%wt increments of the precursor powders. Due to the large overlap of the two precursors' PSDs, the only repeatable blend which produced two mode values was for composition of 75%wt -100 mesh CP Ti which gave a volume frequency percent ratio ($X_L$ / $X_S$) of 1 / 1.

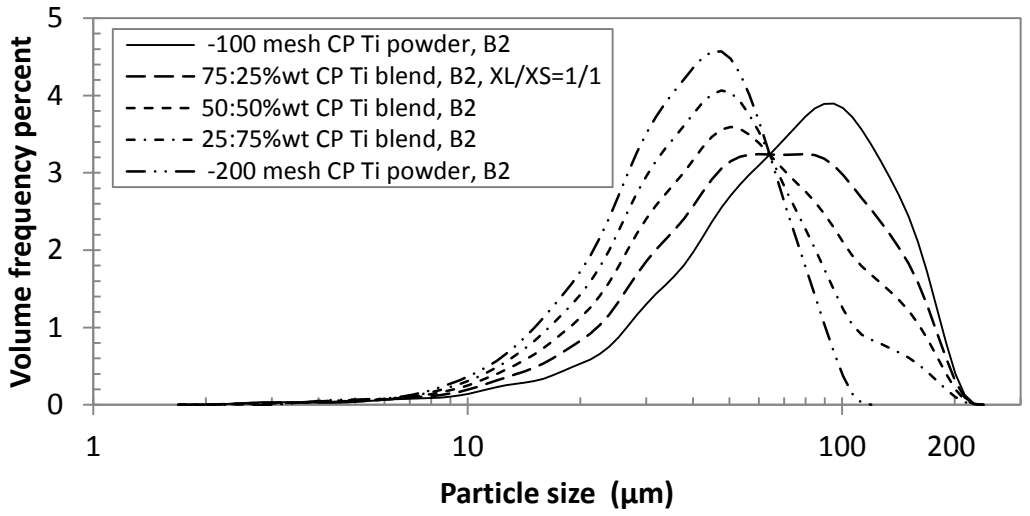


**Figure 31: PSDs of CP titanium blends, B2**

Note that -100 and -200 mesh precursor powders (B2) greatly overlap each other and their mode particle sizes are closer together compared the first batch (B1). This influences both the mode particle sizes of the blends produced, as can be seen in Table 12.

**Table 12: CP titanium blends' PSD characteristics, B2**

| %wt | $D_{10}$ (µm) | $D_{50}$ (µm) | $D_{90}$ (µm) | Mode $X_S$ | Mode $X_L$ | Freq. $X_L$ / $X_S$ |
|---|---|---|---|---|---|---|
| **0:100%wt** | 17.1 | 38.2 | 67.5 | 47.6 | - | - |
| **25:75%wt** | 18.4 | 43.0 | 89.5 | 47.6 | - | - |
| **50:50%wt** | 20.2 | 49.8 | 115.0 | 50.4 | - | - |
| **75:25%wt** | 23.0 | 59.9 | 129.7 | 63.5 | 75.4 | 1 / 1 |
| **100:0%wt** | 27.8 | 72.5 | 138.8 | - | 95.0 | - |

Note: The blends' particle sizes were predicted using precursor powders' measured PSD data.

## 4.6. Preparation of MA Ti-6Al-4V powder blends

The first round of MA Ti-6Al-4V blends (B1) were tailored to have specific frequency percent ratios between the mode values, i.e. the PSD's local peaks, $X_L$ / $X_S$, were specified ratios, as in section 4.5 the ratios chosen were: 1 / 1, 2 / 3, and 1 / 3.

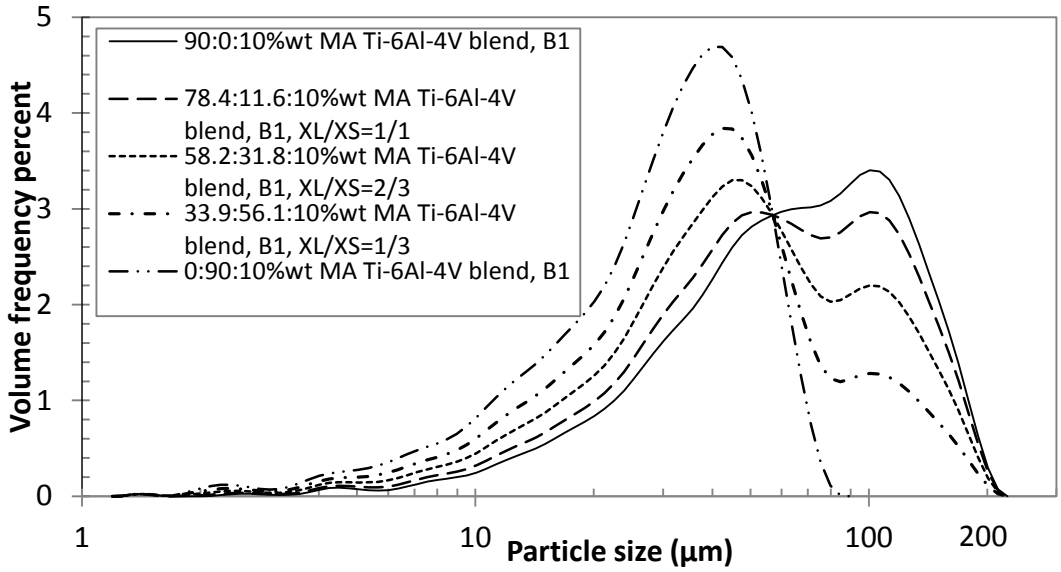


**Figure 32: PSDs of MA Ti-6Al-4V blends, B1**

Similar to the first round of the CP titanium blends, notice that as the %wt -100 mesh increases the $X_S$ peak shifts to the right, i.e. the mode value would be found at a slightly larger particle size, as can be seen in Figure 32 and Table 13.

**Table 13: MA Ti-6Al-4V blends' PSD characteristics, B1**

| %wt | D10 (µm) | D50 (µm) | D90 (µm) | Mode $X_S$ | Mode $X_L$ | Freq. $X_L$ / $X_S$ |
|---|---|---|---|---|---|---|
| **0:90:10%wt** | 10.8 | 31.4 | 53.2 | 40.1 | - | - |
| **33.9:56.1:10%wt** | 13.0 | 38.0 | 97.8 | 42.4 | 100.6 | 1 / 3 |
| **58.2:31.8:10%wt** | 15.5 | 46.0 | 118.5 | 47.6 | 100.6 | 2 / 3 |
| **78.4:11.6:10%wt** | 18.8 | 56.4 | 128.6 | 50.4 | 100.6 | 1 / 1 |
| **90:0:10%wt** | 21.5 | 63.7 | 132.8 | - | 100.6 | - |

Note: The blends' particles sizes were predicted from precursor PSD data.

The second round of Ti-6Al-4V blends prepared consisted of the precursor titanium powders (B2) combined with the master alloy. Due to the large overlap of the two precursors' PSDs, the only repeatable blend which produced two mode values was the composition of 84%wt -100 mesh CP Ti which gave a $X_L$ / $X_S$ ratio of 1 / 1.

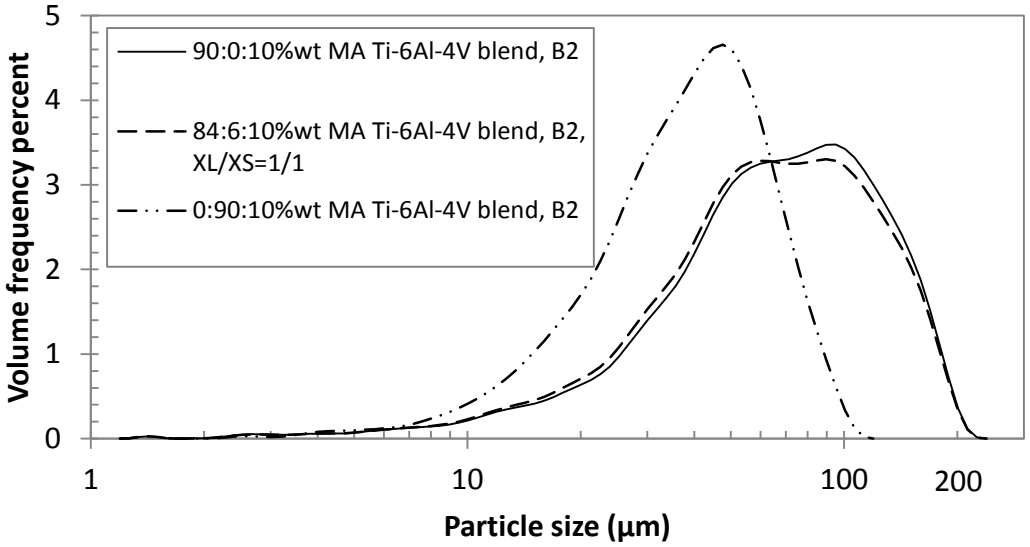


**Figure 33 PSDs of MA Ti-6Al-4V blends, B2**

Due to the results attained from the first batch of MA blends, the scope of second batch was reduced to include only this one blend; this is discussed to a greater extent in section 5.

**Table 14: MA Ti-6Al-4V blends' PSD characteristics, B2**

| %wt | D10 (µm) | D50 (µm) | D90 (µm) | Mode $X_S$ | Mode $X_L$ | Freq. $X_L$ / $X_S$ |
|---|---|---|---|---|---|---|
| **0:90:10%wt** | 16.2 | 38.2 | 66.5 | 47.6 | - | - |
| **84:6:10%wt** | 22.8 | 63.2 | 133.1 | 59.9 | 89.7 | 1 / 1 |
| **90:0:10%wt** | 24.0 | 66.2 | 135.3 | - | 94.9 | - |

Note: The blends' particles sizes were predicted from precursor PSD data.

## 4.7. Powder blends densification pathways

To understand the influence of a powder's PSD on the densification during compaction and sintering, experiments were conducted with the CP and MA blends described in sections 4.5 and 4.6, respectively. These experiments included the production of sintered compacts produced under a range of production parameters which included: compaction pressure, aspect ratio, sintering time and sintering temperature.

### 4.7.1. Densification of CP titanium powder blends

Titanium blends (B1), as described in section 4.5, were pressed at 350, 400, and 450 MPa to form a set of square cylindrical specimens which were sintered at 1300°C for 2 hours.

Titanium blends (B2), as described in section 4.5, were pressed at 400 MPa to form a set of square cylindrical (AR=1:1) and thin disc (AR=1:3) specimens, as shown in Figure 35 and Figure 36, respectively. These specimens were sintered at 1300°C for 2 hour increments, for a maximum sintering time of 6 hours.

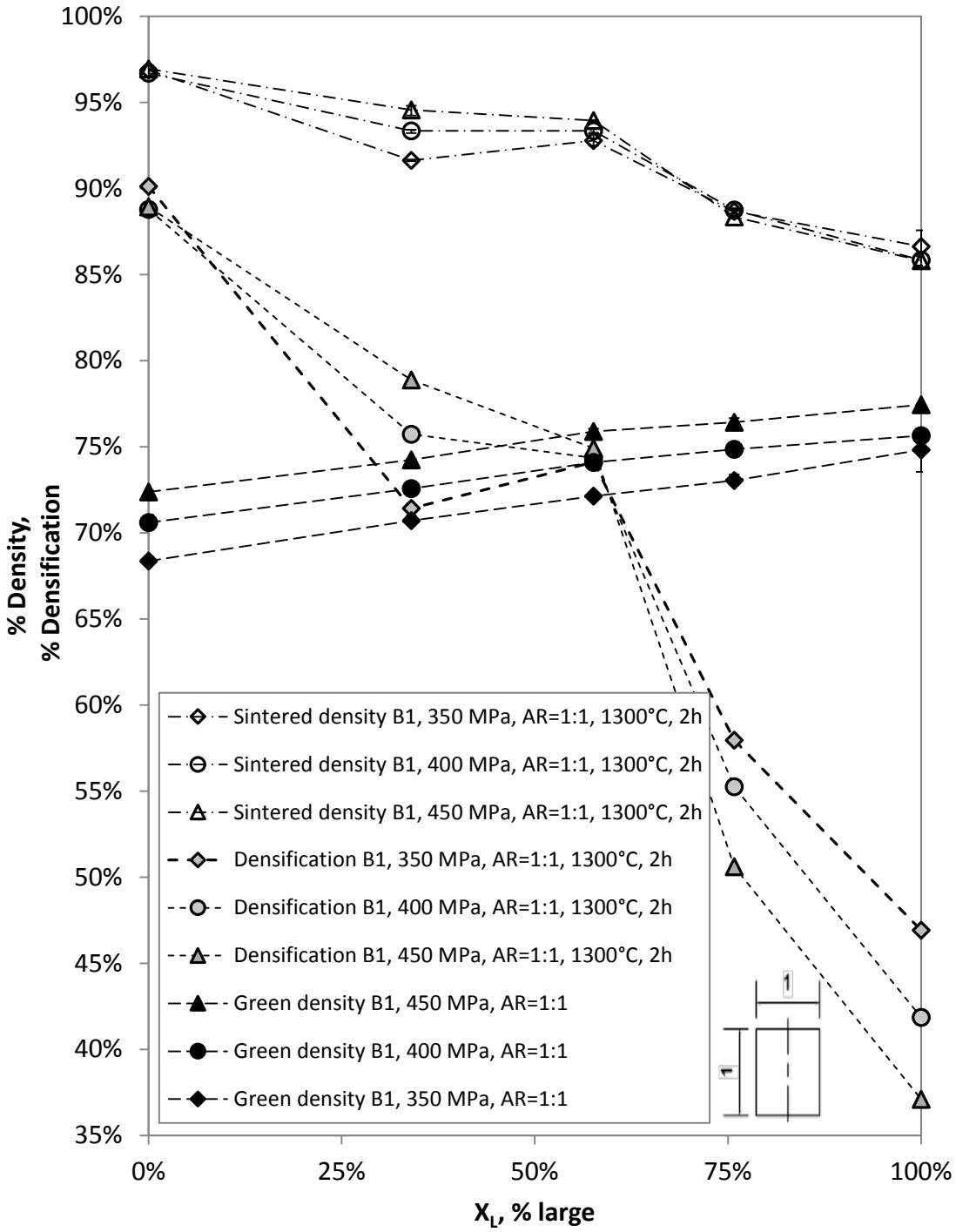


**Figure 34: Influence of compaction pressure on the densification of square cylinders pressed from CP Ti blends, B1 (AR=1:1, sintered at 1300°C, 2 h)**

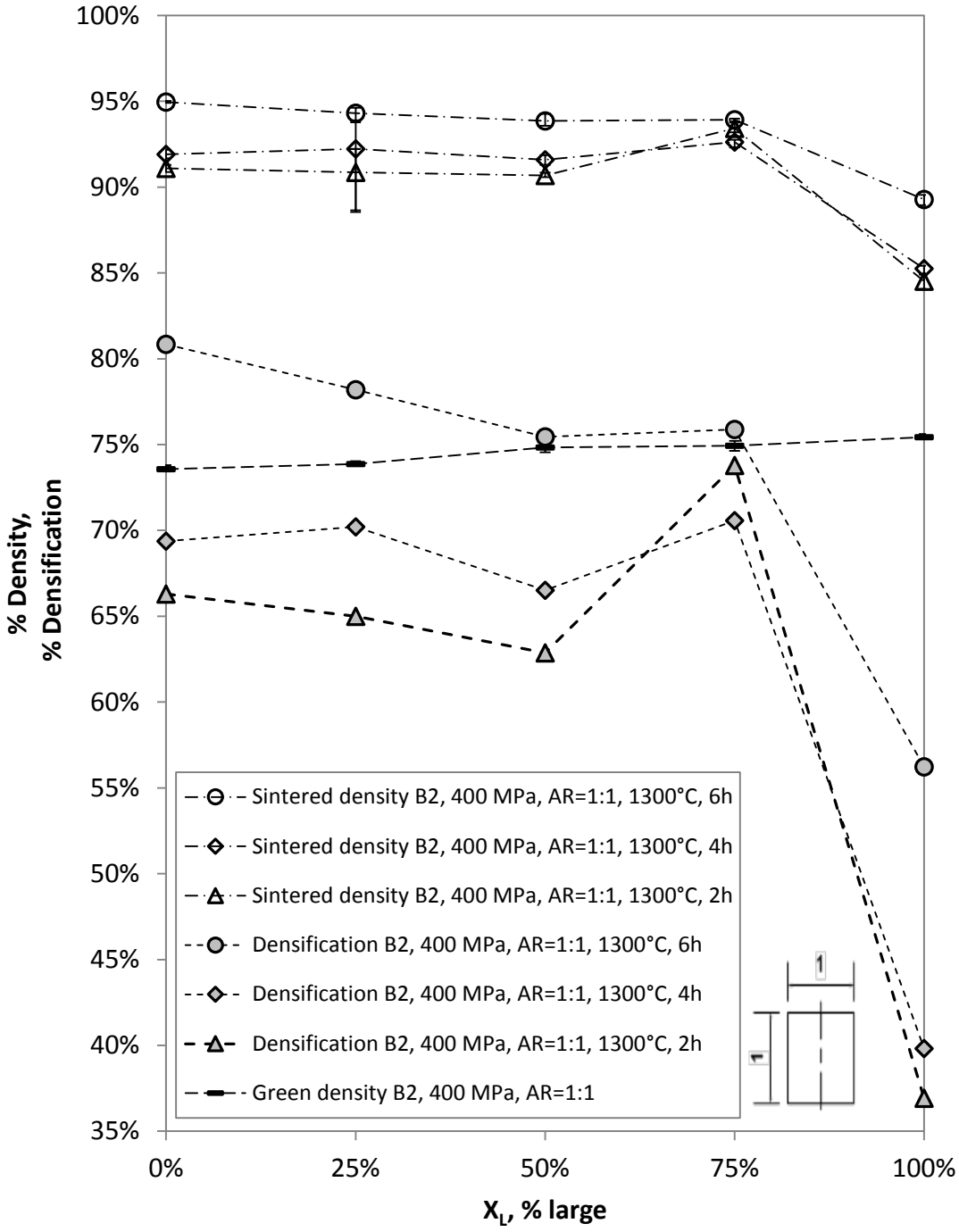


**Figure 35: Influence of sintering time on the densification of square cylinders pressed from CP Ti blends, B1 (compacted at 400 MPa, AR=1:1, sintered at 1300°C for 2, 4, 6 h)**

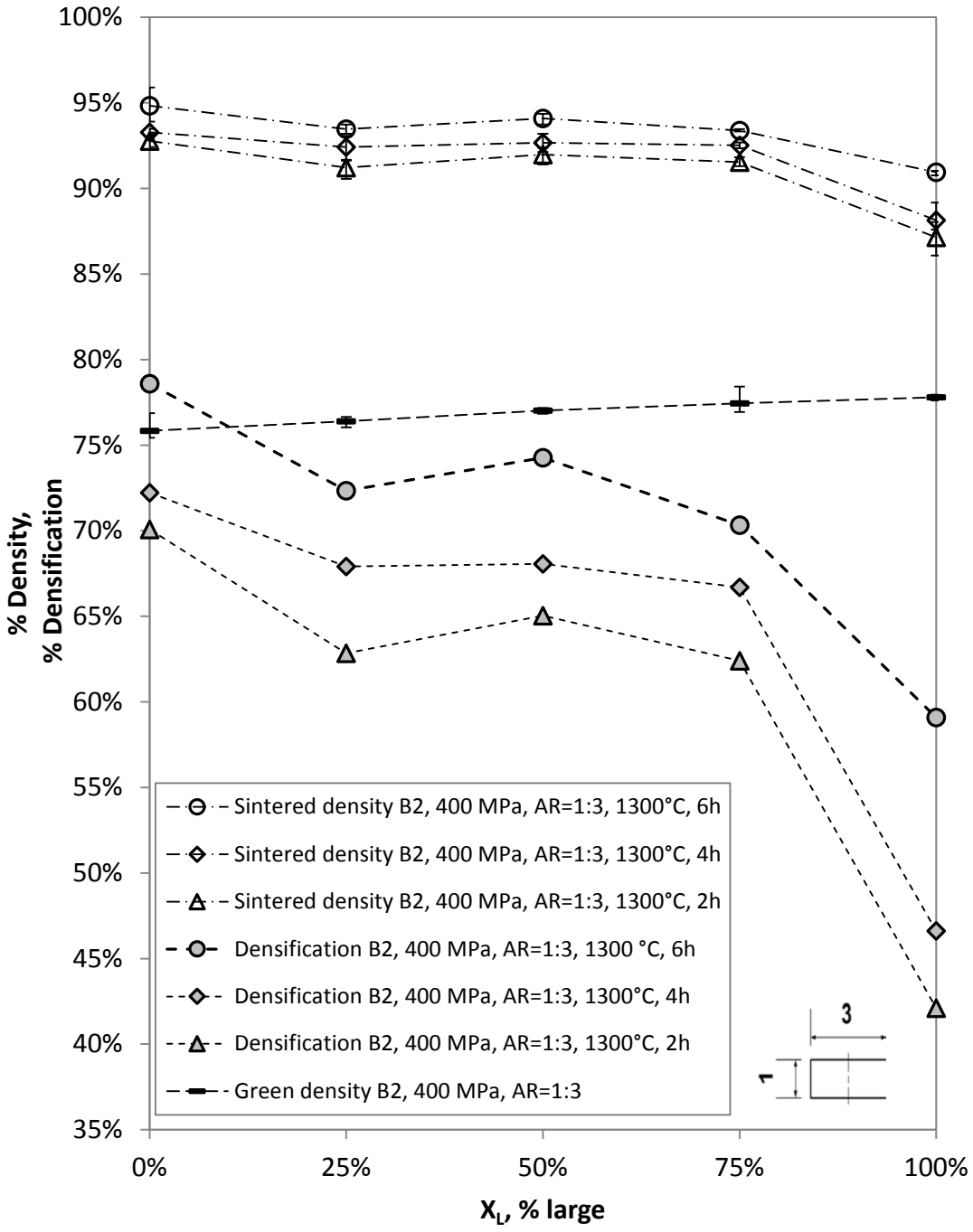


**Figure 36: Influence of sintering time on the densification of thin disk specimens pressed from CP Ti blends, B1 (compacted at 400 MPa, AR=1:3, sintered at 1300°C for 2, 4, 6 h)**

For the purposes of comparison of the titanium blends' densification, the specimens pressed at 400 MPa and sintered at 1300°C for 2 hours were plotted together, as seen in Figure 37.

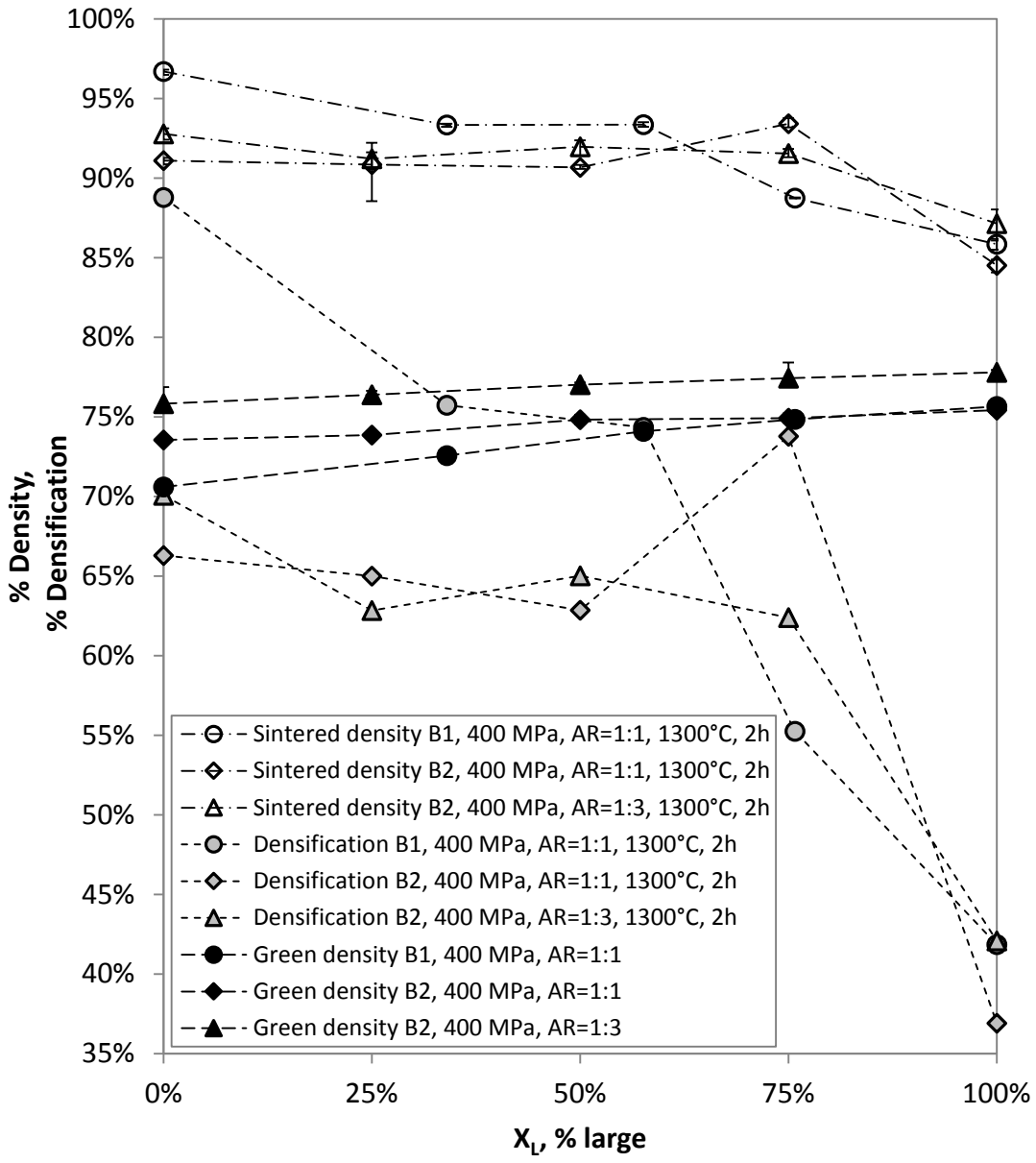


**Figure 37: Comparison of CP Ti blends' densification, B1 and B2 (compacted at 400 MPa, sintered at 1300°C for 2 h)**

### 4.7.2. Densification of MA Ti–6Al–4V powder blends

Master alloy Ti–6Al–4V blends (B1), as described in section 4.6, were pressed at 350, 400, and 450 MPa to form a set of square cylindrical specimens which were sintered at 1300°C for 2 hours.

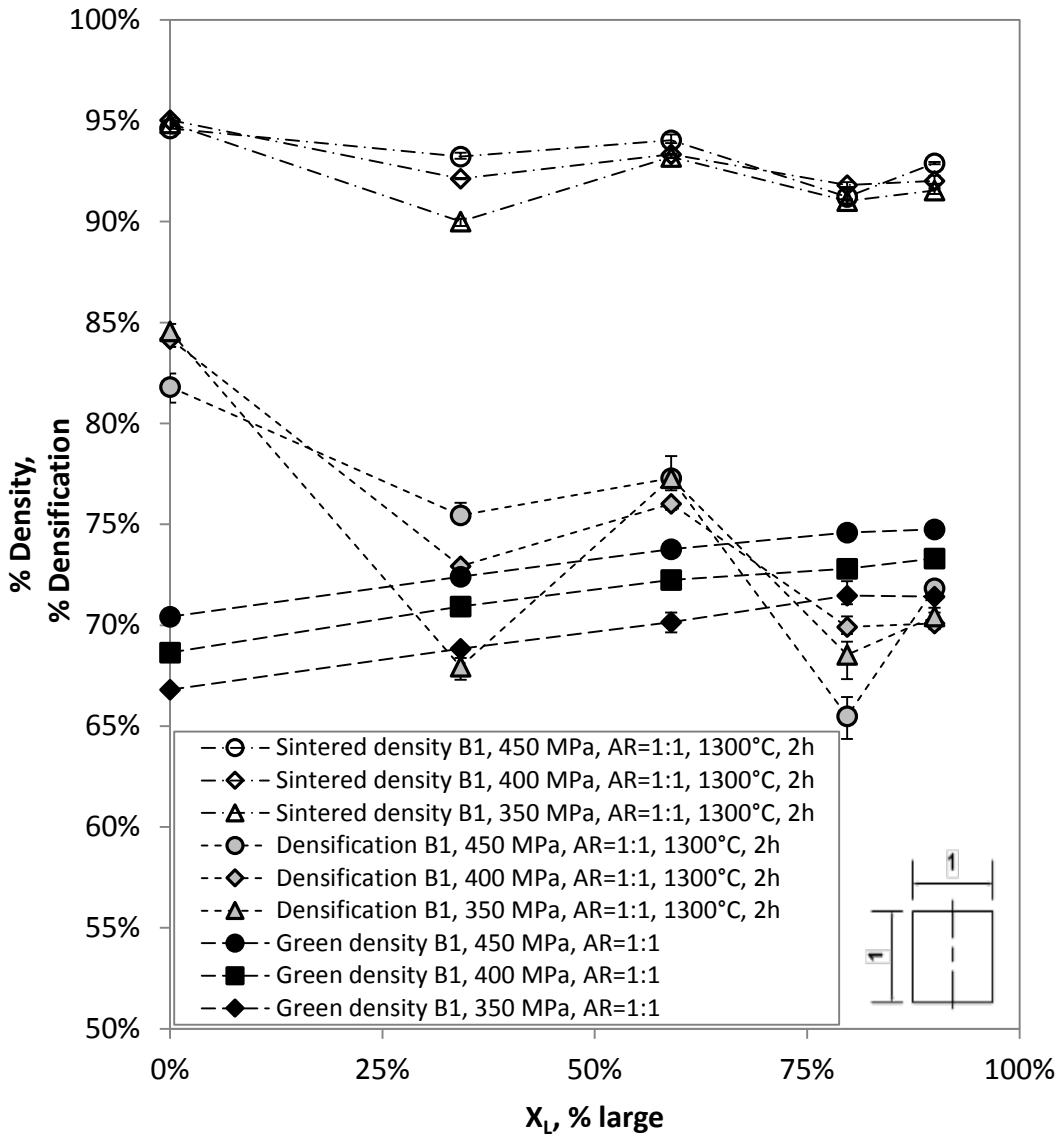


**Figure 38: Influence of compaction pressure on the densification of square cylinders pressed from MA Ti–6Al–4V blends, B1 (AR=1:1, sintered at 1300°C, 2 h)**

Master alloy Ti–6Al–4V blends (B2), as described in section 4.6, were pressed at 400 MPa to form a set of square (AR=1:1) and thin disc (AR=1:3) specimens. These specimens were sintered at 1300°C for 2 hours.

For the purposes of comparison of the Ti–6Al–4V blends' densification, the specimens pressed at 400 MPa and sintered at 1300°C for 2 hours were plotted together on Figure 39.

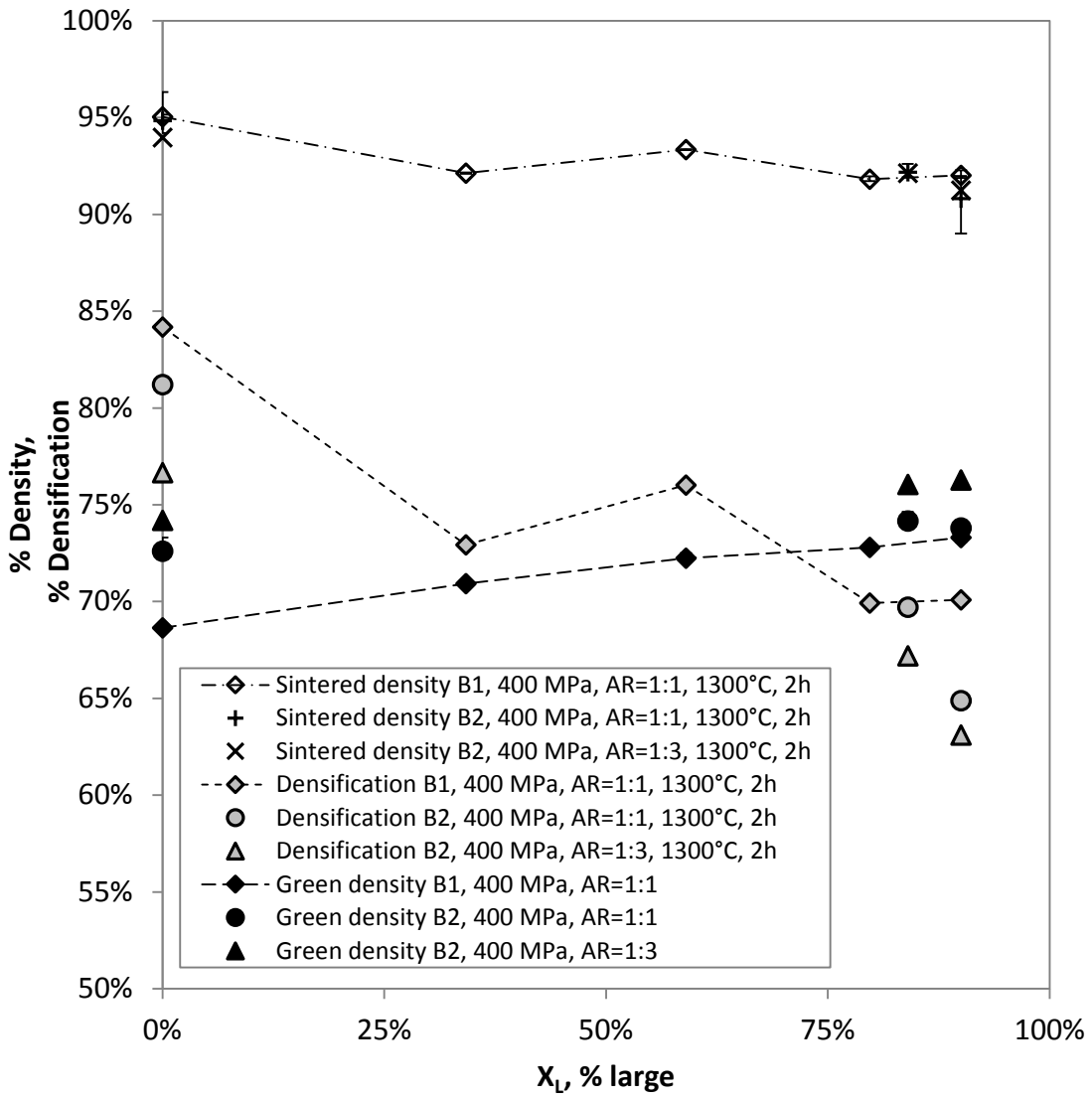


**Figure 39: Comparison of MA Ti–6Al–4V blends' densification, B1 and B2 (compacted at 400 MPa, sintered at 1300°C, 2 h)**

## 4.8. Strength and hardness

To understand the influence of a powder's PSD on the strength and hardness the mechanical testing procedures, as set out in section 3.6, had to be followed. Experiments were to be conducted with the CP titanium and MA Ti-6Al-4V powder blends produced from the second batch of CP titanium precursor powders (B2), as described in sections 4.5 and 4.6, respectively.

Transverse rupture bar (TRB) and thin disk specimens were produced from the CP titanium and MA Ti-6Al-4V (B2) blends, compacted at 400 MPa and sintered at 1300°C. TRBs in both the green and sintered states were tested. The thin disk specimens were produced toward attaining hardness data.

**Table 15: Mechanical properties of CP Ti and MA Ti-6Al-4V blends, TRBs pressed at 400 MPa and sintered at 1300°C, 2 h,**

| Powder | Composition | Relative green density | Green strength (MPa) | Relative sintered density | Elastic modulus (GPa) | Transverse yield stress (0.2% strain, (MPa) | Transverse rupture stress (MPa) | Vickers hardness HV10 |
|---|---|---|---|---|---|---|---|---|
| **CP Ti B2** | 0:100%wt | 75.3% | 27.2 | 93.5% | 37.0 | 815 | 1345 | 177 |
| **CP Ti B2** | 25:75%wt | 76.2% | 33.4 | 91.2% | 33.8 | 737 | 1120 | 169 |
| **CP Ti B2** | 50:50%wt | 75.9% | 28.8 | 92.8% | 35.4 | 725 | 1207 | 157 |
| **CP Ti B2** | 75:25%wt | 76.5% | 30.9 | 92.1% | 33.9 | 674 | 1109 | 151 |
| **CP Ti B2** | 100:0%wt | 77.0% | 31.3 | 89.6% | 30.8 | 600 | 943 | 130 |
| **MA Ti-6Al-4V B2** | 0:90:10%wt | 73.7% | 23.3 | 92.8% | 40.1 | 1361 | 2013 | 271 |
| **MA Ti-6Al-4V B2** | 84:6:10%wt | 75.0% | 24.2 | 92.5% | 38.7 | 1253 | 1590 | 234 |
| **MA Ti-6Al-4V B2** | 90:0:10%wt | 75.6% | 23.8 | 89.1% | 33.6 | 1050 | 1388 | 244 |

It is important to note that the failure mode found in results shown in Table 15 exhibited ductile failure as the midplane deflection greatly exceeding 0.5 mm in all of the specimens subjected to the transverse rupture testing.

The composition of CP titanium blends (B2) were considered with respect to green strength and green density achieved in TRB specimens pressed at 400 MPa.

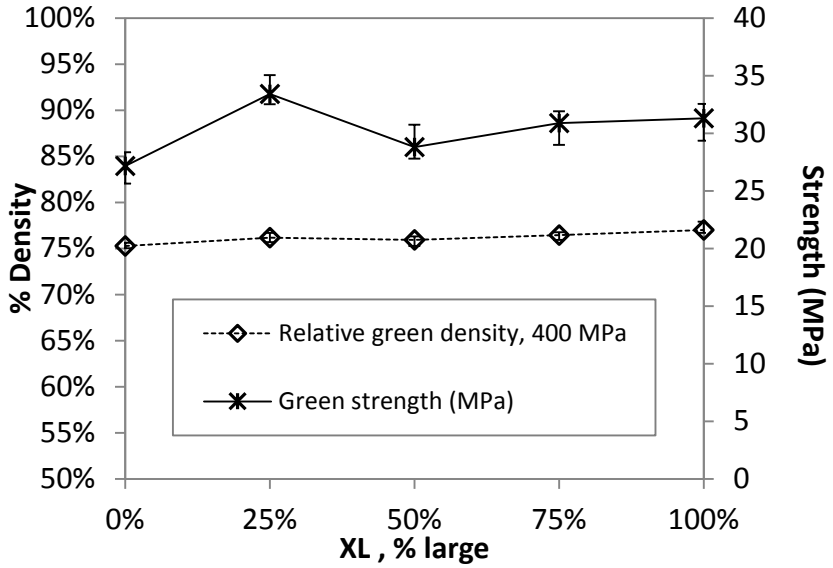


**Figure 40: TRB green density and green strength of CP Ti blends, B2**

Furthermore, the composition of CP titanium blends (B2) were considered with respect to sintered strength and sintered density achieved in TRB specimens pressed at 400 MPa and sintered under vacuum at 1300°C for 2 hours.

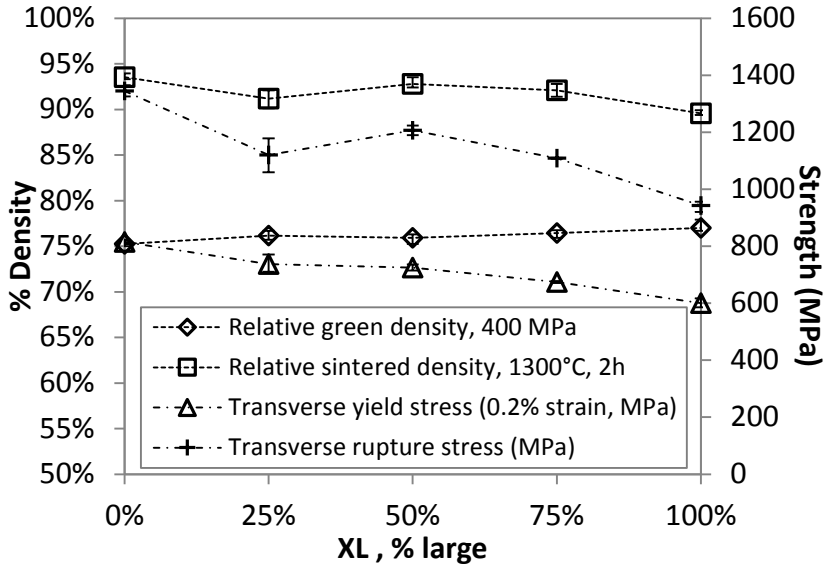


**Figure 41: TRB green and sintered density, YS and TRS, of CP Ti blends, B2**

In an attempt to gain insight into the increase in strength from the green state to the sintered state brought about by sintering, a TRB and thin disc specimens were pressed from the precursor powders (B2) at 400 MPa and sintered at 1000°C for 2 hours. This was done to show increase of sintered strength gained during the early stages of densification.

**Table 16: Densification and mechanical properties of TRBs pressed at 400 MPa and sintered at 1000°C, 2 h**

| Powder | Composition | Relative green density | Green strength (MPa) | Relative sintered density | Elastic modulus (GPa) | Transverse rupture stress (MPa) | Vickers hardness HV10 |
|---|---|---|---|---|---|---|---|
| **CP Ti B2** | 0:100%wt | 75.3% | 27.2 | 85.6% | 29.6 | 958 | 134 |
| **CP Ti B2** | 100:0%wt | 77.0% | 31.3 | 82.6% | 24.6 | 653 | 112 |
| **MA Ti-6Al-4V B2** | 0:90:10%wt | 73.7% | 23.3 | 84.3% | 26.6 | 737 | 186 |
| **MA Ti-6Al-4V B2** | 90:0:10%wt | 75.6% | 23.8 | 81.0% | 22.1 | 519 | 161 |

Contrary to the results in shown Table 15, that the failure mode found in results shown in Table 16 exhibited brittle failure as the midplane deflection did not exceed 0.5 mm in any of the these specimens subjected to the transverse rupture testing.

## 4.9. Thermal conductivity

In preparation for this set of experiments, Ø25.4 mm specimens were pressed at 400 MPa and sintered, with density captured in both states. Temperature data captured during the experiments were sampled at 1 Hz with the power supplied to the cartridge heater and cooling fan held constant, 50 W (60 V DC, ~0.8 A) and 1 W (9 V DC, ~0.1 A) respectively. Conductivity values were calculated from the average of two minutes of steady state temperature data.

**Table 17: Thermal conductivity of specimens sintered at 1300°C, 2 h**

| Powder | Composition | Relative green density | Relative sintered density | Thermal conductivity (W/mK) |
|---|---|---|---|---|
| **CP Ti B2** | 0:100%wt | 75.1% | 91.1% | 10.7 |
| **CP Ti B2** | 100:0%wt | 76.5% | 86.2% | 8.7 |
| **MA Ti-6Al-4V B2** | 0:90:10%wt | 73.2% | 93.0% | 4.0 |
| **MA Ti-6Al-4V B2** | 90:0:10%wt | 75.9% | 91.9% | 4.1 |

**Table 18: Thermal conductivity of specimens sintered at 1000°C, 2 h**

| Powder | Composition | Relative green density | Relative sintered density | Thermal conductivity (W/mK) |
|---|---|---|---|---|
| **CP Ti B2** | 0:100%wt | 74.5% | 74.6% | 3.9 |
| **CP Ti B2** | 100:0%wt | 76.5% | 81.7% | 9.2 |
| **MA Ti-6Al-4V B2** | 0:90:10%wt | 75.4% | 89.1% | 3.8 |
| **MA Ti-6Al-4V B2** | 90:0:10%wt | 73.8% | 83.4% | 2.4 |

## 4.10. Microscopy

Once the densification trends of the CP titanium and MA Ti-6Al-4V powder blends were established, the resulting sintered pore structures were to be examined using optical light microscopy following the procedure outlined in section 3.8. Specimens of CP titanium blends were to be investigated regarding pore size and shape with compaction and sintering parameters were held at 400 MPa and 1300°C for 2 h, respectively; these micrographs can be found in Table 19.

Additional specimens of precursor CP titanium powders and MA Ti-6Al-4V were sintered at 1000°C for 2 h to accompany the strength and hardness results, as reported in section 4.8. These specimens had been prepared in an attempt to gain insight into the evolution of the pore shape during the early stages of sintering. These micrographs can be found in Table 20.

**Table 19: Micrographs of CP titanium pressed at 400 MPa and sintered at 1300°C, 2 h**

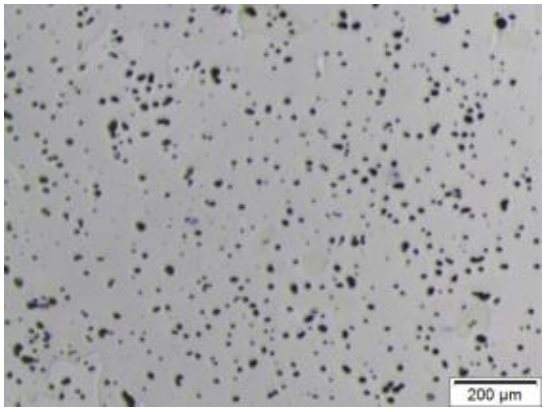


**Figure 42: -200 mesh CP Ti, B1, AR=1:1, 96.9% sintered density**

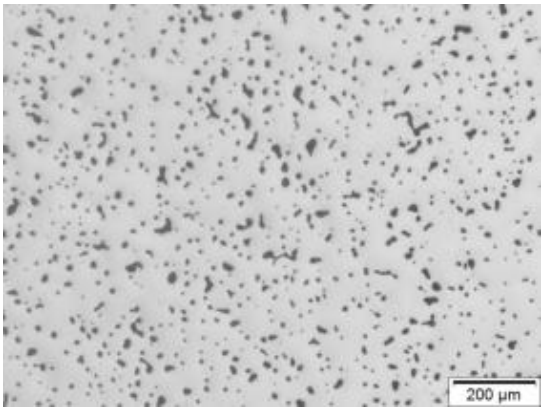


**Figure 43: -200 mesh CP Ti, B2, AR=1:3, 91.1% sintered density**

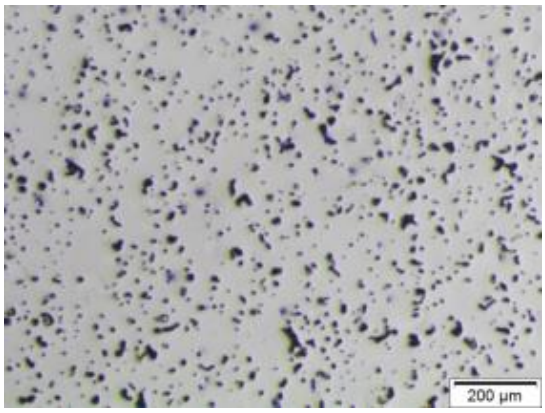


**Figure 44: 34.0:66.0%wt CP Ti blend, B1, AR=1:1, 94.6% sintered density**

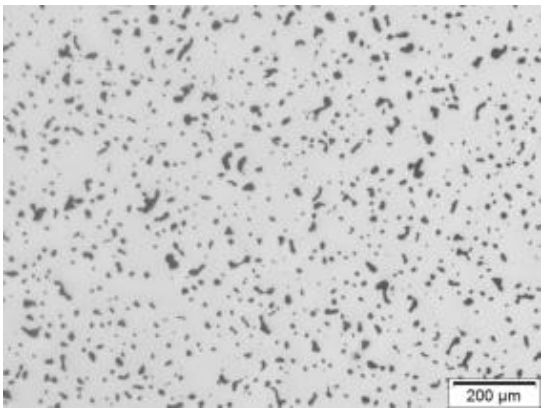


**Figure 45: 25:75%wt CP Ti blend, B2, AR=1:3, 90.9% sintered density**

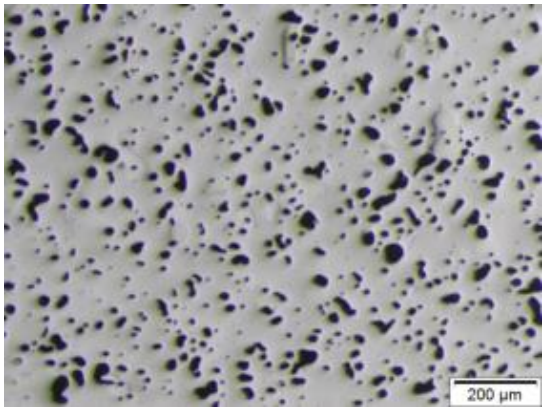


**Figure 46: 57.6:42.4%wt CP Ti blend, B1, AR=1:1, 94.0% sintered density**

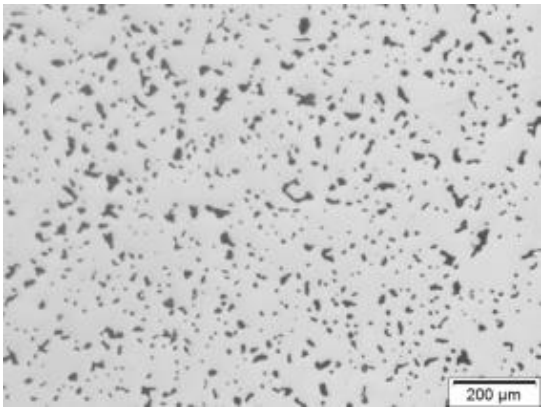


**Figure 47: 50:50%wt CP Ti blend, B2, AR=1:3, 90.7% sintered density**

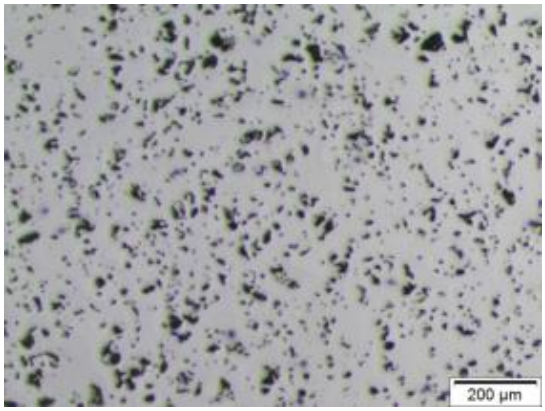


**Figure 48: 75.8:24.2%wt CP Ti blend, B1, AR=1:1, 88.8% sintered density**

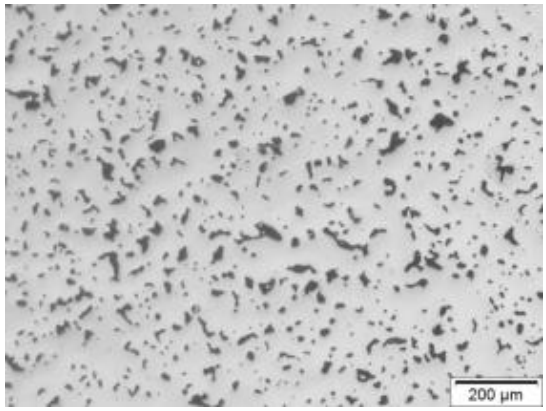


**Figure 49: 75:25%wt CP Ti blend, B2, AR=1:3, 93.4% sintered density**

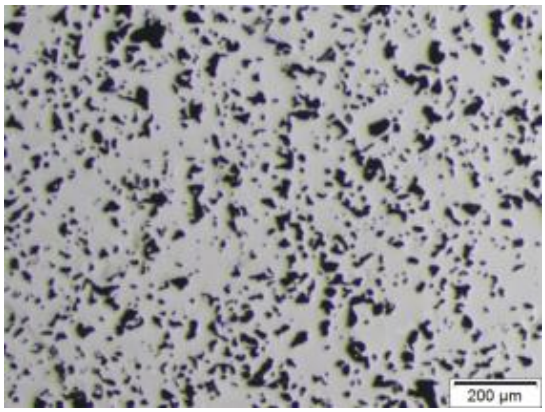


**Figure 50: -100 mesh CP Ti, B1, AR=1:1, 85.8% sintered density**

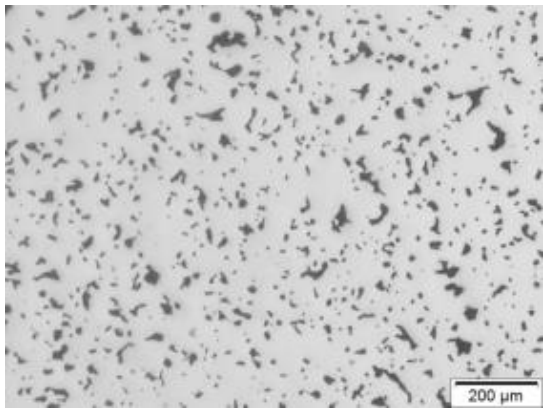


**Figure 51: -100 mesh CP Ti, B2, AR=1:3, 84.5% sintered density**

**Table 20: Micrographs of CP titanium and MA Ti-6Al-4V pressed at 400 MPa and sintered at 1000°C, 2 h**

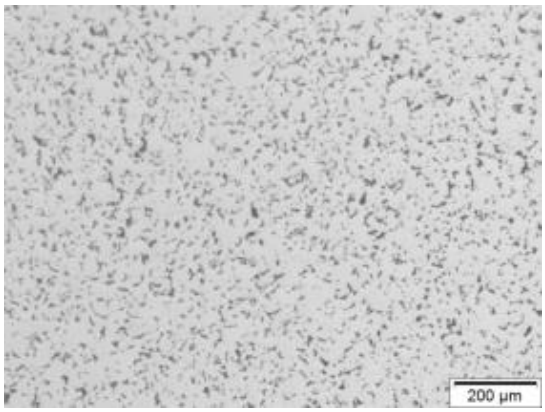


**Figure 52: -200 mesh CP Ti, B2, AR=1:3, 84.1% sintered density**

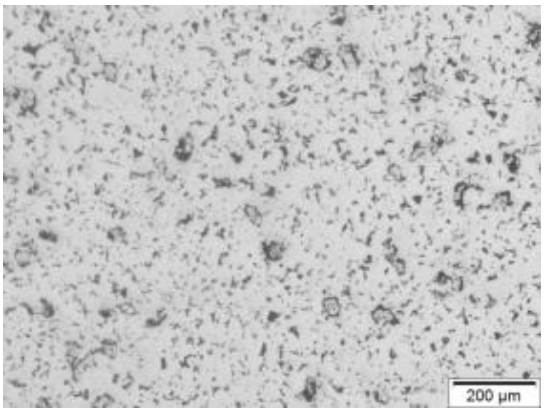


**Figure 53: 0:90:10%wt MA Ti-6Al-4V, B2, AR=1:3, 85.6% sintered density**

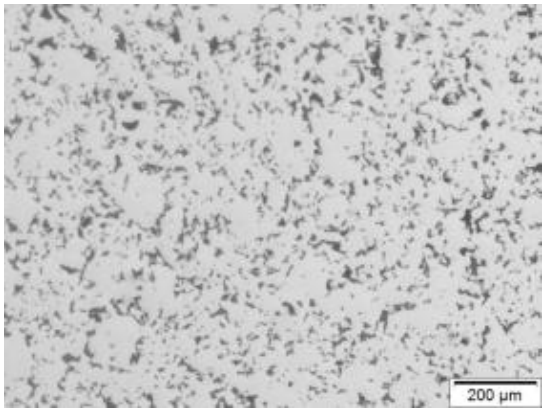


**Figure 54: -100 mesh CP Ti, B2, AR=1:3, 82.1% sintered density**

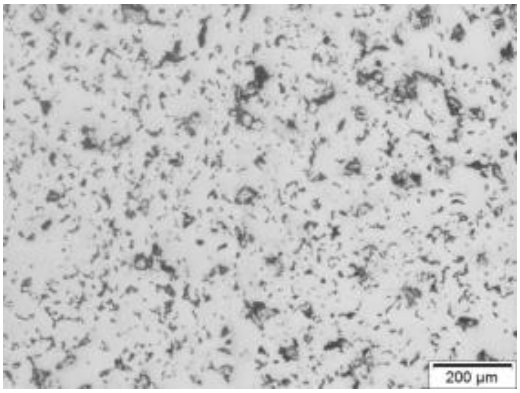


**Figure 55: 90:0:10%wt MA Ti-6Al-4V, B2, AR=1:3, 83.3% sintered density**

# 5. Discussion

A discussion of the results gathered is presented by providing an overview of the densification, mechanical, thermal and microstructural properties, respectively.

## 5.1. Densification of precursor powders and powder blends

When one considers the densification data captured in section 4.3 and 4.7 in a manner similar to that presented in Robertson & Schaffer's work [31], i.e. as shown in Figure 9, plotting the green and sintered densities achieved in relation to lines of constant densification; one's ability to interpret these results becomes improved.

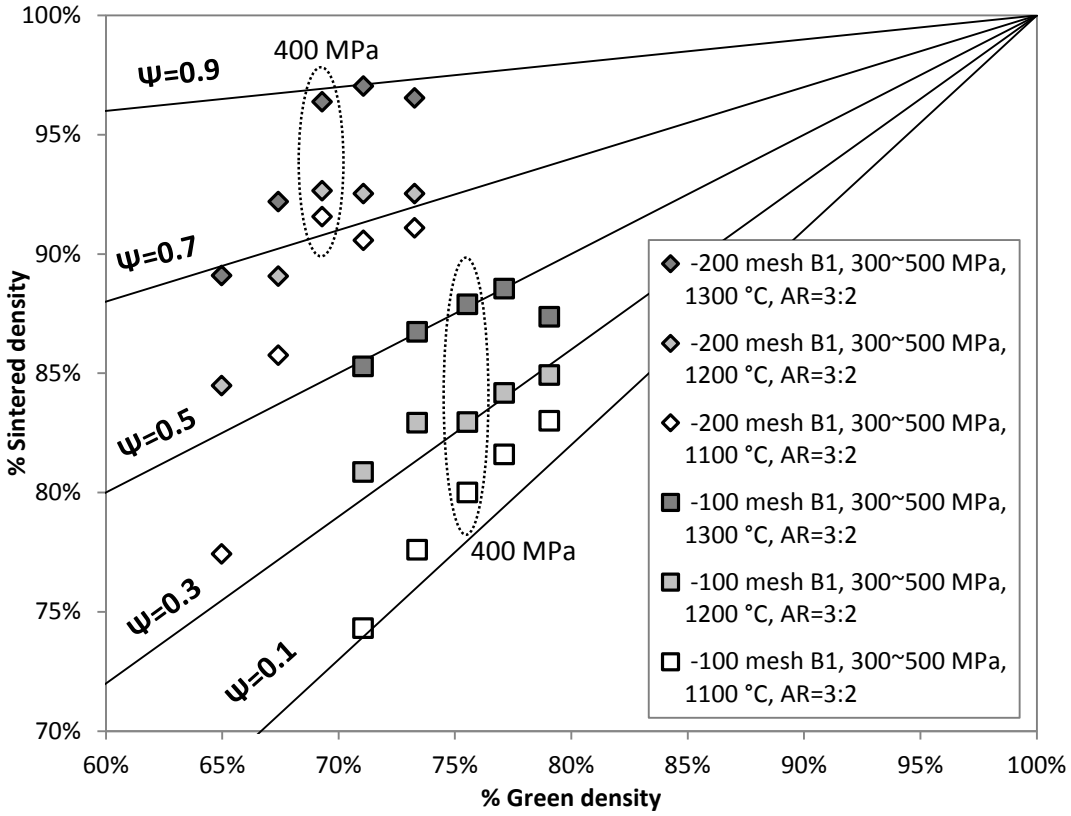


**Figure 56: CP titanium B1 precursor powders densification results plotted alongside lines of constant densification**

Densification of the of the precursor titanium powders in press-and-sinter approach was scrutinized. The effect of increased compaction pressure and sintering temperature on the densification of -100 mesh powders tends to increase linearly along lines of constant densification as evidenced by Figure 56 and Figure 57.

The same can be said of the -200 mesh CP titanium powders, but only within the compaction pressures of 400~500 MPa (B1) and 300~500 MPa (B2) for the respective batches of precursor powders.

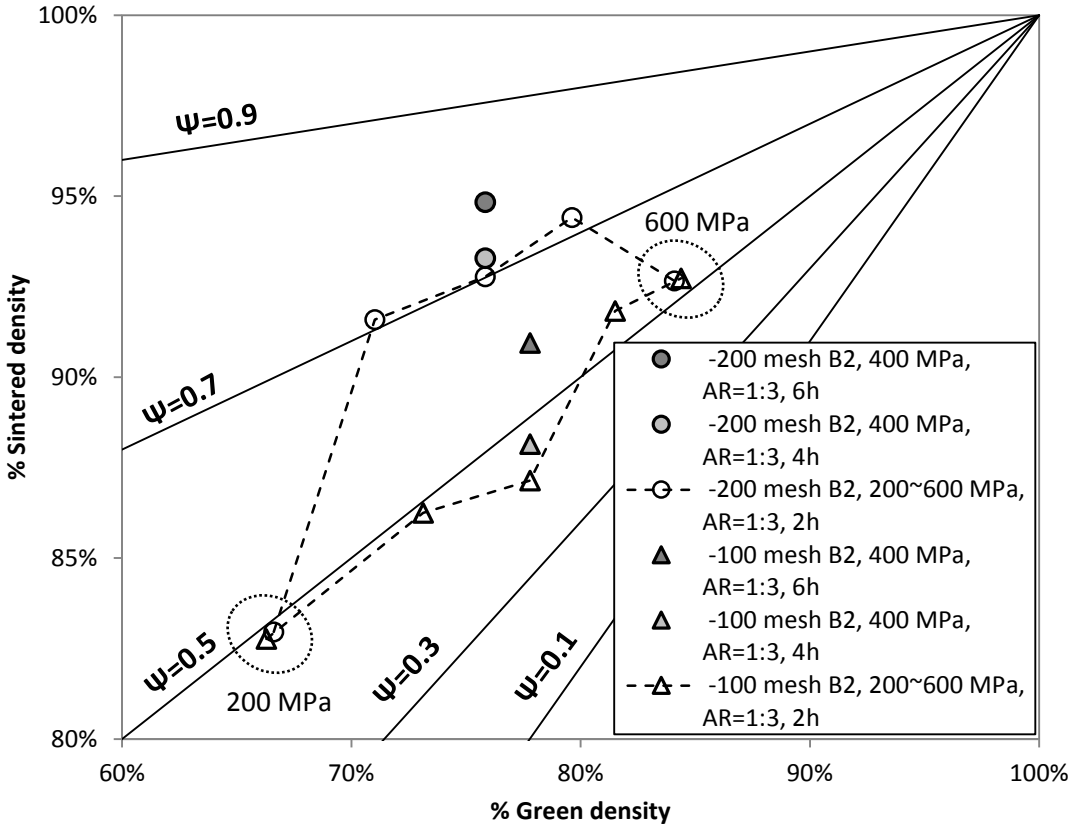


**Figure 57: CP titanium B2 precursor powders densification results plotted alongside lines of constant densification**

The results of the CP titanium blends were also plotted in this manner to show the effect of the ranges of blend compositions on densification behaviour, as presented in Figure 55 and 56.

Note that square cylinder specimens tested (AR=1:1) 75%wt blend produced superior densification relative to the precursors and other blends, which was not evident in the thin disc (AR=1:3) specimens. This effect does call into question the accuracy of the density calculation of the thin disc specimens as the limitation of the measurements taken could have failed to describe the specimens shape with sufficient accuracy. Substrate adhesion sintering defects became noticeable on these thin disc specimens after being sintered for 4 and 6 hours.

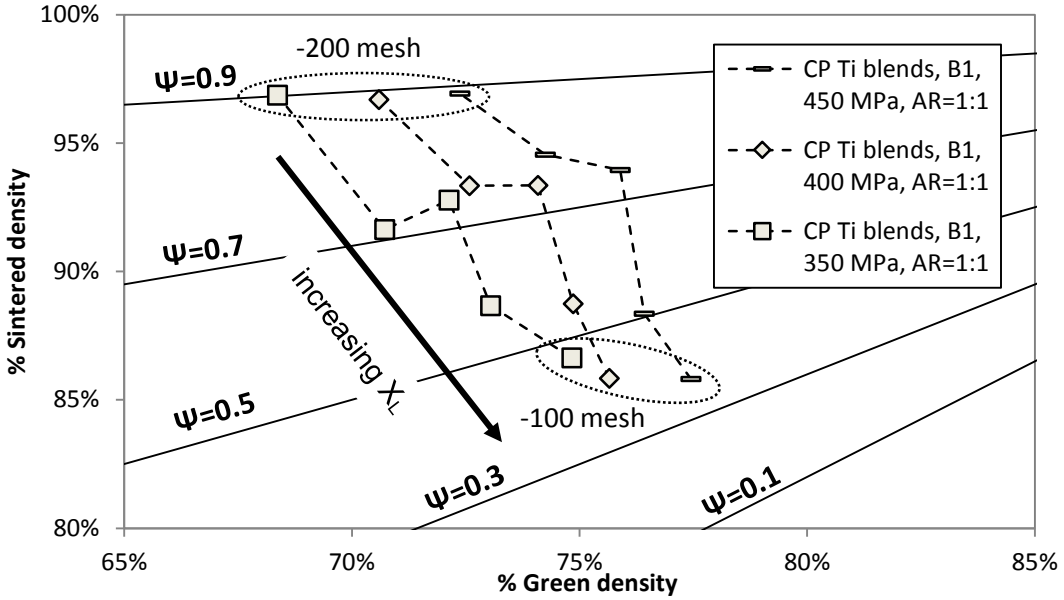


**Figure 58: CP titanium B1 blends' densification results plotted alongside lines of constant densification**

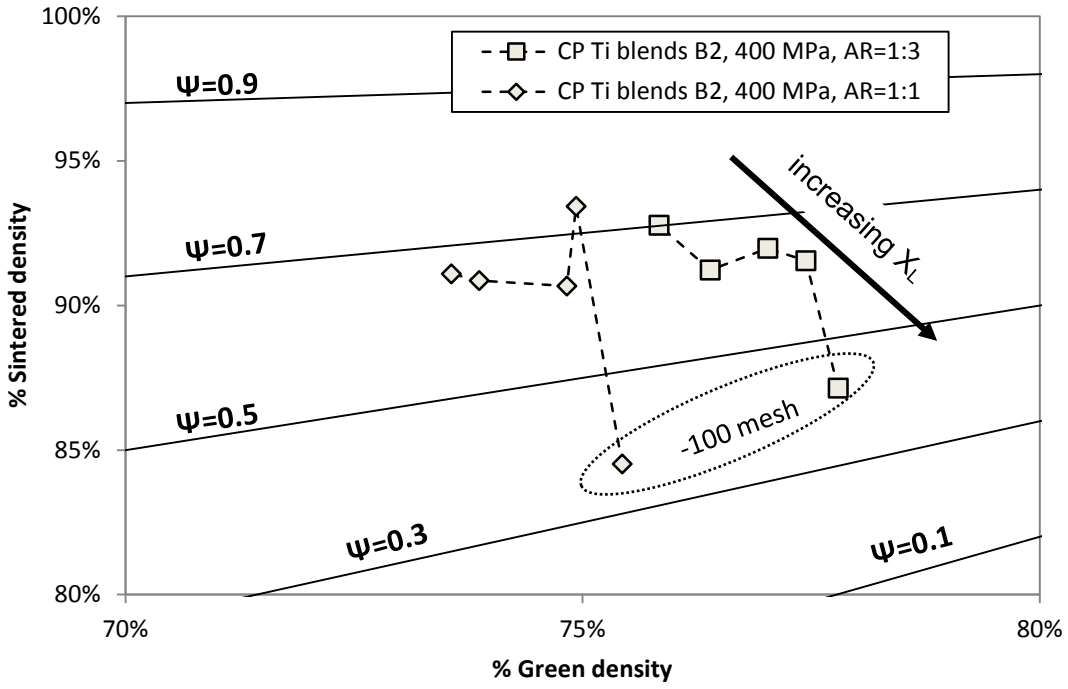


**Figure 59: CP titanium B2 blends' densification results plotted alongside lines of constant densification**

## 5.2. Strength and hardness

CP titanium specimens tested exhibited peak green strength at 25:75%wt blend, see Figure 40, and sintered strength peaked at the 50:50%wt point, see Figure 41. When one compares that to the trend in the TRS and sintered density it becomes apparent that the 25:75%wt blend has greater powder interlocking in the green state, however the sintering potential of the fine powders has a stronger influence in driving densification and thus increasing sintered strength. Sintered hardness, elastic modulus and yield strength tended to follow the variation in sintered density.

Specimens vacuum sintered at 1300°C for 2 hours exhibited ductile fracture which renders the data gathered to only be of comparative value, as the displacements were beyond the scope of the test used. Conversely specimens sintered at 1000°C (2h) did fracture in a brittle fashion; furthermore, the MA specimens underperformed the CP when the sintering temperature was lowered.

## 5.3. Thermal conductivity

The conductivity tests yielded mixed results if one compares the captured data to that found in literature. The improvements made to the conductivity testing apparatus, as described in section 3.7 were successful; however the heat input remained somewhat underpowered.

Despite this, the setup did manage to capture some useful data when driven at the maximum input power (60 V DC). The data, as seen in Table 21 and Table 22, reflects relatively poor thermal conductivity of PM titanium, less than half relative to their wrought equivalents.

It is noteworthy that the -100 mesh CP titanium specimen's conductivity did not increase with an increase in sintering temperature.

**Table 21: CP Titanium specimens' thermal conductivity results**

| Material | Sintering temperature | Relative density | Conductivity |
|---|---|---|---|
| **Titanium** | Wrought | 100% | 22 W/m.°C [14] |
| **-100 mesh CP Ti** | 1000°C | 81.7% | 9.2 W/m.°C |
| **-100 mesh CP Ti** | 1300°C | 86.2% | 8.7 W/m.°C |
| **-200 mesh CP Ti** | 1000°C | 77.6% | 3.9 W/m.°C |
| **-200 mesh CP Ti** | 1300°C | 91.1% | 10.7 W/m.°C |

**Table 22: MA Ti-6Al-4V specimens' thermal conductivity results**

| Material | Sintering temperature | Relative density | Conductivity |
|---|---|---|---|
| **Ti-6Al-4V** | Wrought | 100% | 8 W/m.°C [14] |
| **0:90:10%wt MA** | 1000°C | 89.1% | 3.8 W/m.°C |
| **0:90:10%wt MA** | 1300°C | 93.0% | 4.0 W/m.°C |
| **90:0:10%wt MA** | 1000°C | 83.4% | 2.4 W/m.°C |
| **90:0:10%wt MA** | 1300°C | 91.9% | 4.1 W/m.°C |

## 5.4. Microscopy

The micrographs gathered in section 4.10, one can deduce that the CP titanium blends produced sintered pore structure's become coarser with an increase in the -100 mesh powder.

The reduction of pore size and number of pores, together with pores becoming more rounded can be attributed to the increasing addition of smaller particles which enhances sintering rate, allowing sooner onset of final stage sintering and improved final sintered density. However, it has proven cumbersome to accurately quantify using optical light microscopy due to the exposed surface's tendency to smear during metallographic preparation.

Thus another means of investigation, namely computed tomography (CT) scanning, was explored as part of the collaborative work of Fester [23], however the details of that endeavour falls outside the scope of this document.

# 6. Conclusions

This body of work continued from the endeavours of Laubscher [9], among others [7, 8, 10, 13], and approach used was greatly influence by the work of Robertson and Schaffer [30, 31, 32].

The densification data pertaining to the –100 and –200 mesh precursor CP titanium powders, as collected by Laubscher [9] were expanded. Variation in compaction pressure, aspect ratio, sintering time and temperature were considered. The trends in collected data suggested that suitable degree of densification could be achieved through pressing at 400 MPa followed by vacuum sintering at 1300°C for 2 hours. Thus, the prepared blends were subjected to these production parameters. An additional set of precursor specimens where pressed at 400 MPa sintered at 1000°C for 2 hours for comparative purposes.

CP Titanium and MA Ti–6Al–4V powder blends of a predictable particle size distribution (PSD) were blended. Specimens were prepared to seek out their PSDs' effect on densification. The effects of particle size distributions for a range of titanium and Ti–6Al–4V powder blends on the green and sintered densities were investigated. This effect of the PSDs on densification was shown to be significant in the with the exception of the sintered density of the Ti–6Al–4V where the MA powder addition's effect on sintering was dominant. Green density was shown to increase as the mean particle became larger; conversely the sintered density achieved was variant depending on composition. The CP titanium PSDs' effect was noted to display some bimodal characteristics, especially around the 75%wt $X_L$ point where enhanced densification was noted, which is in line with trends found in literature [14]. As for the MA Ti–6Al–4V blends, this effect on sintered density was not was not distinctive.

The relationship between the densification pathway and the mechanical, thermal and microstructural properties was also investigated.

Ductile titanium and Ti–6Al–4V TRB specimens were produced through press-and-sinter densification pathway: pressed at 400 MPa and sintered at 1300°C for 2 hours. Specimens sintered at 1000°C for 2 hours exhibited brittle behaviour. Hardness and yield strength tended to increase as the PSD became smaller, yet the variation in TRS and sintered density were noted to be similar.

Thermal conductivity properties were attained using a modified version of the apparatus developed by Combrink [7] and Coetzer [8]. The conclusion of these tests suggests that PM titanium and Ti–6Al–4V have poor conductivity properties relative to their wrought equivalents; but this test method and experimental setup requires further refinement.

The microstructural properties investigated were limited to that of the sintered pore structures. Pore structure micrographs have been presented and show the relative pore size and shape. Problems arose the repeatability in the metallographic surface preparation of the various specimens had been prevalent. Thus an alternative Computed Tomography (CT) scanning method was investigated in collaboration with Fester [23]; however, this was outside of the scope for this body of work and thus omitted from this report. Similarly, the production of stepped cylinders as developed by Sobiyi [13] was pressed at GKN, in conjunction with the work done by Fester [23], but as a suitable set of test specimens could not be attained.

Thus the following recommendations stem from these conclusions:

CP titanium powder stocks of -100, -200 and -325 mesh should be considered in future work. This would allow for a wider range of the PSDs to become achievable. Attaining detail chemical composition of the powder makeup would also be recommended to account for impurity content.

Microstructural examination, including phase and grain size analysis in addition to chemical homogeneity, should be undertaken to understand the relations between sintered microstructure and sintered strength with respect to sintering temperature.

Tooling capable of producing tensile specimens through the press-and-sinter method should be procured. The transverse rupture tests conducted as part of this research has shown ductile behaviour and thus prompt this action.

The thermal conductivity apparatus' heating probe should be fitted to a high temperature heat source. It would be the author's recommendation mount the heating probe to interior of a muffle furnace via a feedthrough on the furnace door. This would allow greater control and higher heat flow through the apparatus. Furthermore, test specimens should be compared to the data captured of the corresponding wrought equivalent.

Processing of further densification test specimens through the press-and-sinter techniques should be considered in square cylinder aspect ratio. Specimens are subjected to the Archimedes density test and in addition to CT techniques. This would allow for a two benefits, a greater understanding of the error involved when capturing density data by physical measurement and theoretical density calculation; and secondly, the influence of specimen's density gradient on densification.

## References

[1] Seong S, Younossi O, Goldsmith BW, Lang W, Neumann M. Titanium, Industrial Base, Price Trends, and Technology Initiatives. RAND Corporation, 2009.

[2] Klug KL, Ucok I, Gungor MN, Guclu M, et al. The Near-Net-Shape Manufacturing of Affordable Titanium Components for the M777 Lightweight Howitzer. JOM, November 2004, pg.35-41.

[3] Qian M. Cold Compaction and Sintering of Titanium and Its Alloys for Near-Net-Shape or Preform Fabrication. International Journal of Powder Metallurgy, 2010, Volume 46, Issue 5, p.29

[4] Peter WH, Blue CA, Scory CR, Ernst W, McKernan JM, Kiggans JO, Rivard JDK, Yu C. Non-Melt Processing of “Low-Cost”, Armstrong Titanium and Titanium Alloy Powders. 2007. Proceedings of the Light Metals Technology (LMT) Conference, 2007.

[5] Jackson M, Dring K. A Review of Advances in Processing and Metallurgy of Titanium Alloys. Materials Science and Technology, 2006, Vol 22, No 8, p.881.

[6] Standard Test Methods for Metal Powders and Powder Metallurgy Products – 2010 Edition. Metal Powder Industries Federation (MPIF). Princeton: MPIF; 2010.

[7] Combrink JH. The correlation between thermal conductivity and porosity in sintered titanium. [Bachelors dissertation]. Stellenbosch: SUN; 2012.

[8] Coetzer JA. Modelling stresses during machining of sintered titanium. [Bachelors dissertation]. Stellenbosch: SUN; 2013.

[9] Laubscher HH. Press-and-sinter processing of HDH Ti powder. [Bachelors dissertation]. Stellenbosch: SUN; 2012.

[10] Clinning NJ. A study of the densification and microstructural evolution of blended elemental Ti–6Al–4V during hot deformation. [Masters dissertation]. Cape Town: UCT, 2012.

[11] Bedinger GM. US Geological Survey Minerals Yearbook - 2012: Titanium. September 2014.

[12] Bedinger GM. US Geological Survey, Mineral Commodity Summaries: Titanium Mineral Concentrates, January 2015.

[13] Sobiyi KK. Machining of powder metal titanium. [Masters dissertation]. Stellenbosch: SUN; 2012.

[14] German RM. Sintering Theory and Practice. New York: Wiley-Interscience Publication; 1996.

[15] Titanium information group, datasheets [online] [s.a] [access 2014, February]; Available: http://www.titaniuminfogroup.co.uk/data-sheets

[16] Cengel YA, Ghajar, AJ. Heat and Mass Transfer. New York: McGraw-Hill; 2011.

[17] Froes FH, Friedrich H, Kiese J, Bergoint D. Titanium in the Family Automobile: The Cost Challenge. JOM, February 2004, p.40-44.

[18] Kuczynski GC. Self-diffusion in Sintering of Metallic Particles. Metals Transactions, February 1949.

[19] G.C. Kuczynski. The Mechanism of Densification during Sintering of Metallic Particles. Acta Metallurgica, January 1956, Vol 4, p.58.

[20] German RM. Powder Metallurgy & Particulate Materials Processing. Princeton: MPIF; 2005

[21] German RM. Coarsening in Sintering: Grain Shape Distribution, Grain Size Distribution, and Grain Growth Kinetics in Solid-Pore Systems. Critical Reviews in Solid State and Materials Sciences, 2010, 35:263–305.

[22] Alexander BH, Balluffi RW. The Mechanism of Sintering Copper. Acta Metallurgica, November 1957, Vol 5, p.666.

[23] Fester AL. Evaluating and reducing density gradients and defects in die compacted powder parts. [Bachelors dissertation]. Stellenbosch: SUN; 2014.

[24] F.H. Froes, S.J. Mashl, V.S. Moxson, J.C. Hebeisen, and V.A. Duz. The Technologies of Titanium Powder Metallurgy. JOM, November 2004, p.46.

[25] McCracken CG, Motchenbacher C, Barbis DP. Review of titanium powder production methods. International Journal of Powder Metallurgy, 2010, Volume 46, Issue 5, p.19

[26] Whittaker D. Titanium powders for mass production, general engineering applications. International Powder Metallurgy Directory. [Online] [Accessed Feb 2012]; Available: http://www.ipmd.net/

[27] Moxson VS, Senkov ON, Froes FH. Production and Application of Low Cost Titanium Powder Products. The International Journal of Powder Metallurgy, 1998, Vol 3, No.5, p.45

[28] Arcella FC, and Froes FH. Producing Titanium Aerospace Components from Powder using Laser Forming. JOM, May 2000, p.28-30.

[29] German RM. Sintering densification for powder mixtures of varying distribution widths. Acta metall, mater. Vol. 40, No. 9, pp. 2085-2089, 1992.

[30] Robertson IM, Schaffer GB. Review of densification of titanium based powder systems in press and sinter processing, 53(2). Powder Metallurgy, 2010, Vol 53 No 2, p.146.

[31] Robertson IM, Schaffer GB. Some Effects of Particle Size on the Sintering of Titanium and a Master Sintering Curve Model. Metallurgical and materials transactions A, Volume 41A, November 2010, 2949-2958.

[32] Robertson IM, Schaffer GB. Refinement of Master Densification Curves for Sintering of Titanium. Metallurgical and materials transactions A, Volume 41A, November 2010, 2949-2958.

[33] Standard Test Method for Apparent Density of Free-Flowing Metal Powders Using the Hall Flowmeter Funnel, ASTM International, B212-13. Baltimore: ASTM International; 2013.

[34] Standard practices for the production and preparation of powder metallurgy (P/M) test specimens, ASTM International, B925-03. Baltimore: ASTM International; 2003.

[35] Standard test method for compressibility of metal powders in uniaxial compression, ASTM International, B331-95. Baltimore: ASTM International; 2002.

[36] Standard Test Method for Transverse Rupture Strength of Powder Metallurgy (PM) Specimens. ASTM International, B528-05. Baltimore: ASTM International; 2005.

[37] Standard test method for measuring dimensional changes of metal powder specimens, ASTM International, B610-00. Baltimore: ASTM International; 2001.

[38] Standard test method for density, oil content, and interconnected porosity of sintered metal structural parts and oil impregnated bearings. ASTM International, B328–96. Baltimore: ASTM International; 2003.

[39] Dowling NE. Mechanical Behavior of Materials, New Jersey: Prentice Hall; 2012.

[40] Standard test method for green strength for compacted metal powder specimens, ASTM International, B312–96. Baltimore: ASTM International; 2002.

[41] Metallographic preparation of titanium [Online] [s.a.] [access 2014, August]; Availible: http://www.struers.com/resources/elements/12/282484/Application_Note_Titanium_2014_ENG.pdf

[42] S.H. Anver. Introduction to Physical Metallurgy, 2nd Edition. Michigan: McGraw-Hill, 1974.

[43] Metallographic preparation of powder metallurgy parts [Online] [s.a.] [access 2014, August]; Availible: http://www.struers.co.uk/resources/elements/12/101197/Application%20Notes%20Powder%20Metals%20English.pdf

# Appendix A: Works procedures for PM titanium

# Appendix A1: Works procedure for powder blending

## Scope

This document outlines the works procedure for preparing blends of PM powders. Required materials and equipment are listed together with related maintenance, risk and safety information.

## Materials

Precursor powders, isopropyl alcohol, and paper towels.

## Equipment

PPE: Gloves, particulate mask.

Turbula-type mixer, laboratory scale (±10 mg), scoop, permanent marker, mixing and storage vessels.

## Risk and safety

### Powder

Fine powder dusts are highly flammable, especially when aerated, thus keep away from open flames or sources of heat. Certain materials are dangerous when inhaled/ingested, come into contact with skin/eyes, thus use PPE as appropriate.

### Mixer

Clear area around moving armature, belt drive, electric motor and control unit. Ensure all fixtures and safety covers are tightened down securely, do not operate without the safely covers in place.

## Maintenance

### Powder storage

Store precursor powders and powder blends in a dry and vibration free area.

Ensure the precursor powders and blends are sufficiently blended before use.

### Mixer

Ensure the armature and blending vessel fixtures are in place and tightened down before use. Do not operate the mixer above 30 rpm.

## Operating procedure

Once the blend's by weight composition of precursor powders had been determined and the appropriate mixing and storage vessels have been procured, proceed with the following operating procedure.

### Setup and preparation

1. Clean mixing and storage vessels by washing with alcohol and drying with paper towels.
2. Check the armature and mixer fixtures are secure.
3. Setup mixer control unit and zero speed settings.
4. Setup laboratory scale and clean the platen, zero the read out.

### Work progression

1. Place mixing vessel on lab scale and tare the read out.
2. Scoop the in desired composition of precursor powders into the mixing vessel, ensure the vessel is filled to 30~50% vol. as this will ensure sufficient
3. Ensure the vessel is securely sealed before placing the container in to the mixer.
4. Close the safety hood and allow the mixer to run for 10~20 mins at ~15 rpm.

### Shutdown

Ensure the armature has fully stopped and isolate the power supply before any attempts are made at removing safety covers or removing the mixing vessel.

## Notes

If troubleshooting: seek out documentation from manufacturer and/or assembler.

# Appendix A2: Works procedure for uniaxial cold compaction

## Scope

This document outlines the works procedure for uniaxial cold compaction of powder metallurgical (PM) titanium green compact specimens in free standing toolsets. Required materials and equipment are listed together with related maintenance, risk and safety information.

## Materials

Powder (blend), cotton buds/swabs, weighing paper, zinc stearate, isopropyl alcohol, paper towels, hydraulic oil, and 1 µm Diamond Duo suspension.

## Equipment

PPE: Gloves, safety glasses*, particulate mask*, safety boots*.

Toolset: die, punches, spacer, core- and push-rods*.

Hydraulic press with sufficient force, stroke and platen surface area for compaction.

Measurement equipment: laboratory scale (±10 mg), Vernier callipers (±10 µm) and/or micrometer (±1 µm).

Specimen containers*, permanent marker*, engraver*, funnel*. (*where applicable)

## Risk and safety

### Manual handling injuries

Toolset and hydraulic press components can be sharp and/or cumbersome, thus, use PPE as appropriate and request assistance as required.

### Powder

Fine powder dusts are highly flammable, especially when aerated, thus keep away from open flames or sources of heat. Furthermore, titanium powders are highly reactive with oxygen at high temperatures and result in an exothermic reaction, thus it is imperative to maintain a high vacuum when above 400°C. If a fire does do not use conventional fire extinguisher, rather smother with dry sand.

Particulate materials can be dangerous when inhaled/ingested, come into contact with skin/eyes, thus, use PPE as appropriate.

Hydraulic press

Clear area around the moving platens before and after use. Ensure safe, no-load conditions are reached before manipulating the toolset during compaction cycle.

Toolset

Prolong tool life: keep punch heads and die cavity clean and lubricated.

Avoid compaction pressures above 600 MPa for freestanding toolsets.

Avoid large powder fills that result in high ejection pressures.

Excessive screeching or pinging noises during compaction and ejection cycle can be indicative of toolset damage, inspect surface finish and lubrication.

**Toolset maintenance**

The compaction of PM titanium powder can cause significant damage during ejection if the toolset has not properly been cleaned and lubricated prior to use. Toolset wear is significant when compacting titanium powders and thus sufficient pre-emptive maintenance is required. Regular toolset lubrication is recommended to reduce friction and ease green part ejection; however, accumulated damage can require lapping of the toolset. Both procedures are outlined below together with preparation of die wall lubricant:

**Die wall lubricant preparation**

Add zinc stearate and isopropyl alcohol, in a ratio of 1 g/10 ml, into a sealable vessel and shake vigorously until a milky suspension has formed, free of lumps, use immediately. Separation can occur within an hour, thus continually stir/shake during use to maintain a consistent suspension.

**Toolset lubrication**

Maintaining toolset with sufficient lubrication can prolong tool life and ensure punches and green part can be ejected with minimal friction damage:

1. Clean punch heads and die cavity with cotton wetted with alcohol.
2. Dry punch heads and die cavity with paper towel.
3. Consider pressing a paper specimen to sweep the die wall surface, especially if the different powder (blend) type had been used previously in the toolset.
4. Inspect surface finish: ensure punches achieve a smooth sliding fit throughout stroke in the die cavity, if not refer to “Toolset lapping” procedure below.

5. Apply die wall lubricant cavity and mating punch faces using cotton buds/swabs and allow suspension to dry. An adequate coating should leave a thin white residue of zinc stearate.
6. Wipe off excess lubricant with paper towel, reducing it to a thin sheen.
7. Ensure punches still achieve a smooth sliding fit throughout stroke in the die cavity.

**Toolset lapping**

After prolonged use of a toolset, accumulated friction damage can lead to scoring on die cavity and punch heads. This toolset damage can lead to reduced surface finish quality of green. In extreme cases this can cause the toolset to cease completely, typically the bottom punch would not be retrievable from the die cavity after part ejection. While in operation and difficulties are experienced despite sufficient lubrication, suspend further compaction and lap the toolset.

1. If not yet competed, repeat first four steps from toolset lubrication procedure.
2. Apply a few drops of 1 µm Diamond Duo suspension to the die wall.
3. Stroke bottom punch through the die cavity until a smooth sliding fit is achieved.
4. Repeat step 3 with top punch.
5. Clean punch heads and die cavity with cotton wetted with alcohol.
6. Dry punch heads and die cavity with paper towel.
7. Press a paper specimen to sweep the die wall surface.
8. Inspect surface finish of punch heads and die wall, repeat the Toolset lapping procedure.
9. Proceed with toolset lubrication procedure.

**Operating procedure**

Here follows an outline of the uniaxial compaction procedure toward pressing PM titanium parts.

**Setup and preparation**

<u>Hydraulic press</u>

- Determine the correct conversion between gauge and effective pressures specific to toolset in use.
- Ensure oil levels are sufficient to achieve full stroke, if not consult press's technical documentation and fill reservoir with correct oil grade (contact SMD manager).

- Prepare platens with fixtures for compression, check parallelism and mark out the centre positions for the top and bottom punches to ensure initial toolset alignment.

Digital measuring equipment

- Ensure anvils are clean and zero is held to within the instrument's resolution
- Conduct test measurements by comparing analogue and digital measurements
- If bias is suspected, attain calibration test measures from SMD stores to confirm
- Verify batteries have sufficient charge; if displayed values are dim and/or flashing replace batteries

Powder

- Confirm that a sufficient mass of the correct powder is available.
- Ensure the powder is sufficiently blended to avoid settling and sampling bias.

Toolset

- Unpack, clean and lubricate the toolset.
- Check die and punches' surface finish and sliding fit are acceptable.

**Work progression**

1. Setup lubricated toolset in the filling position <image without/with core rod>.
2. Place weighing paper on scale and tare the measurement.
3. Scoop powder onto the paper to target weight too an acceptable degree of accuracy.
4. Funnel powder into die cavity and level off the fill.
5. Slide top punch into die cavity.
6. Place filled toolset on the hydraulic press platen, centred.
7. Close platens until minimal force is applied to the toolset in single action.
8. Ensure the alignment has remained acceptable.
9. Increased hydraulic pressure to initial compaction pressure is achieved (50~100 MPa).
10. Release pressure in order to remove spacer to achieve the floating die condition.
11. Increased hydraulic pressure to final compaction pressure is achieved (200~600 MPa), hold for ~3 seconds.
12. Release pressure and lower toolset in order to remove top punch.

13. Place spacer on top of the die in position for ejecting the part.
14. Increased hydraulic pressure until part starts to eject.
15. Either hold or slowly increase hydraulic pressure until part is released from die cavity.
16. Release hydraulic pressure and lower platen, retrieve toolset and part from the press.
17. Extract bottom punch from die in order to clean and lubricate die set.
18. Imprint part number on green compact with engraver and place in specimen container.

**Shutdown**

1. Release hydraulic pressure and lower platens.
2. Clean and lubricate toolset before placing into storage.
3. Clean and shut off all equipment before placing into storage.
4. Dispose of all spent materials.
5. Wipe down work area.

**Notes**

Weighing paper can be produced from cutting wax paper into $(50\ mm)^2$ squares.

# Appendix A3: Works procedure for vacuum sintering

## Scope

This document outlines the works procedure for vacuum sintering of powder metallurgical (PM) titanium specimens. Required materials and equipment are listed together with related maintenance, risk and safety information.

## Materials

Specimens to be racked and heated.

## Equipment

Tube furnace fitted with an argon supply and two stage vacuum pump system as developed with the cooperation of Vacutech, together with required PPE and refractory materials:

PPE: Heat resistant gloves, apron, safety boots

Tube furnace

- Elite 1500°C horizontal tube furnace (model: TSH 15-50-180) with alumina tube
- Single program controller (model: EuroTherm 2416)
- Over temperature display (model: EuroTherm 3116)
- Custom made end plates with clamps and seals to act as an interface between both the argon supply and the vacuum system with either end of the tube:
    - End plate with inlet valve to attach the argon supply into the furnace tube
    - End plate with outlet valve to allow the furnace to attach to the vacuum system

Argon supply

- Argon cylinder (Afrox: high purity argon) fitter with regulator
- Regulator pressure valves & gauges to control & display the tank & supply pressures
- Gas flow rate gauge.

Vacuum pump system

- Rotary vane pump, Adixen model: Pascal 2012 SD. (Switch labelled: Backing Pump)
- Turbo pump, Varian model: Turbo-V 81-M. (Switch labelled: Turbo Pump)
- Vacuum gauge, Adixen model: ACS 2000.(Switch labelled: Vacuum Gauge)
- Vacuum accessories: Vac-hoses, clamps, T-pieces, seals, ball valves, particulate filter and non-return valve.

Refractory materials

- Yttria stabilized zirconia crucibles
- Refractory heat shields
- Alumina push rods

**Risk and safety**

The operation of a vacuum furnace can leave the operator and equipment to vulnerable through exposure to high vacuum, electricity, heat, asphyxiation and tripping hazards.

Furthermore, titanium powders are highly reactive with oxygen at high temperatures and result in an exothermic reaction, thus it is imperative to maintain a high vacuum when above 400°C. If a fire does do not use conventional fire extinguisher, rather smother with dry sand.

Vacuum

Exposure of human tissues to high vacuum conditions can cause a gas embolism which, in extreme cases, can be fatal. Thus, never attempt to adjust or loosen hoses or fittings while the vacuum has been drawn or while the vacuum pumps are in operation.

Electrical

Insure all equipment is earthed and do not attempt to make any alterations to the equipment while connected to mains power.

Heat

High furnace temperatures present a serious hazard, ensure area is clear of flammable materials, do not attempt handle any equipment while temperatures are above 300°C.

Ventilation

Argon gas in high concentrations poses an asphyxiation hazard, thus ensure the furnace room is well ventilated especially while flushing the furnace with argon.

Lighting

Ensure work area remains well lit during operation and free of tripping hazards.

**Maintenance**

Tube furnace

Tube's interior requires regular cleaning, hover or sweep tube with paper towel, avoid any sources of moisture or residue. Ensure tube has remained centred relative to the furnace's heating length.

Furnace requires maintenance once the over temperature of the furnace reaches >10°C above the holding temperature (while under steady state conditions), as the thermal insulation and heating coil performance will steadily degrade with use.

Vacuum systems

Require annual servicing or when the system fails to establish high vacuum (~$10^{-5}$ mbar) under no-load/shut-off conditions.

Argon supply

Once cylinder pressure drops below 5 MPa, replace.

**Operating procedure**

Furnace setup and programming, the sintering cycle and system shutdown procedure discussed below. Be sure to fill in a new heat sheet to document the procedure for posterity.

**Setup and preparation**

1. Loosen tube end plates and ensure the tube is free of dust and debris.
2. Place specimens in crucibles, ensure they are well racked <phrasing>.
3. Slide crucibles into the tube using an alumina rod, ensure the crucibles are positioned well within the furnace's heated length.
4. Insert refractory shields on both ends of the tube to contain heat within the heated length.

5. Close off the tube by tightening down the end plates on both the argon supply and vacuum hose side, ensure endplate seals fit concentric and flush to the tube.
6. Ensure the argon inlet valve and regulator valves are closed.

**Argon flushing and vacuum setup**

1. Open argon cylinder valve and throttle the regulator valve to attain a gauge pressure of 50 kPa. Note the cylinder pressure on heat sheet.
2. Switch on the non-return valve in order to open it.
3. Switch on the vacuum pressure gauge, confirm that $P_v > 10^2$ mbar.
4. Adjust gate valves to close high vacuum (HV) line then open low vacuum (LV) line.
5. Switch on the rotary vane pump to allow the tube to be pumped down via the LV line.
6. Once the $Pv < 5 \times 10^{-2}$ mbar, open the argon inlet valve and throttle the flow rate to ~2 L/s resulting in $Pv > \sim 10^2$ mbar. Allow argon to flush through the tube for ~20 min. Note both the flow rate and flush duration on the heat sheet.
7. Close the argon inlet valve, once the $P_v < 10^{-2}$ mbar, note the vacuum pressure achieved on the heat sheet, adjust gate valves to close the LV line, then open the HV line.
8. Switch on the turbo pump, once the $P_v < 10^{-4}$ mbar, proceed with heating procedure. Note the vacuum pressure achieved on the heat sheet.

**Furnace program and heat**

Firstly the operator requires access to edit settings on the controller. This can be done using the “Page”, “Scroll”, ”Set” procedure to get to the page required, enter the code and gain full access: page to “Access List”, scroll to “Pass Code”, set it to “1”; scroll to “Access”, set it to “Full“

Secondly, using the “Page”, “Scroll”, ”Set” procedure, program the controller’s “RAMP”, “DWELL” & “END” phases as per the manufacturer’s manual according to the operator needs.

Thirdly, ensure the controller is set to “HEAT ON” and then “FURNACE RUN”.

Finally monitor the furnace and update the heat sheet at least every 30 min with a new entry containing: time, vacuum pressure and furnace temperatures (over-, element-, and controller temperatures). Once the furnace has cooled to below 300°C (typically overnight), isolate the furnace heating elements and continue with the shutdown procedure.

**Shutdown**

1. Switch off the turbo pump and wait until $P_v$ > 5 x 10-3 mbar, adjust gate valves to close the HV line, then open the LV line. Once the turbo pump has spun down proceed.
2. Open the Argon inlet valve slowly to throttle a flow rate to ~2 L/s resulting in Pv > ~$10^2$ mbar. Allow Argon to backfill the tube for ~10 min.
3. Switch off the rotary vane pump, then adjust gate valves to close the LV line.
4. Close the Argon cylinder valve, wait for the cylinder pressure gauge to zero, then close the regulator and inlet valves.
5. Remove the endplates, first the vacuum system endplate, and remove the argon supply endplate.
6. Slide the crucibles out of the tube using an alumina rod.
7. Allow the tube, specimens and crucibles to cool down fully.
8. Clean tube, replace the endplates.

**Notes**

To sinter under argon, end the “Argon flushing and vacuum setup” at the end of step 6 and start the “Shutdown” at step 2.

To expedite the sintering procedure, program the furnace while the turbo pump spins up.

Vacuum system was supplied by Vacutech and maintained by WCVP. Tube furnace was supplied and maintained by Elite Thermal Systems. Crucible supplied by Ceratech.

[ THIS PAGE HAS BEEN LEFT BLANK DELIBERATELY ]